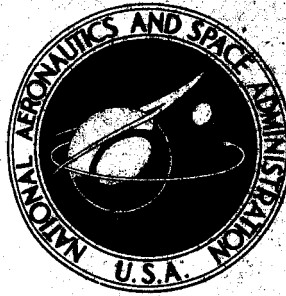


168-16978

**NASA CONTRACTOR  
REPORT**



**NASA CR-991**

NASA CR-991

**CASE FILE  
COPY**

**EXPERIMENTAL INVESTIGATION OF FLOW  
PATTERNS IN RADIAL-OUTFLOW VORTEXES  
USING A ROTATING-PERIPHERAL-WALL  
WATER VORTEX TUBE**

*by Arthur Travers*

*Prepared by*  
**UNITED AIRCRAFT CORPORATION**  
East Hartford, Conn.

*for*

**NATIONAL AERONAUTICS AND SPACE ADMINISTRATION • WASHINGTON, D. C. • FEBRUARY 1968**

EXPERIMENTAL INVESTIGATION OF FLOW PATTERNS  
IN RADIAL-OUTFLOW VORTEXES USING  
A ROTATING-PERIPHERAL-WALL WATER VORTEX TUBE

By Arthur Travers

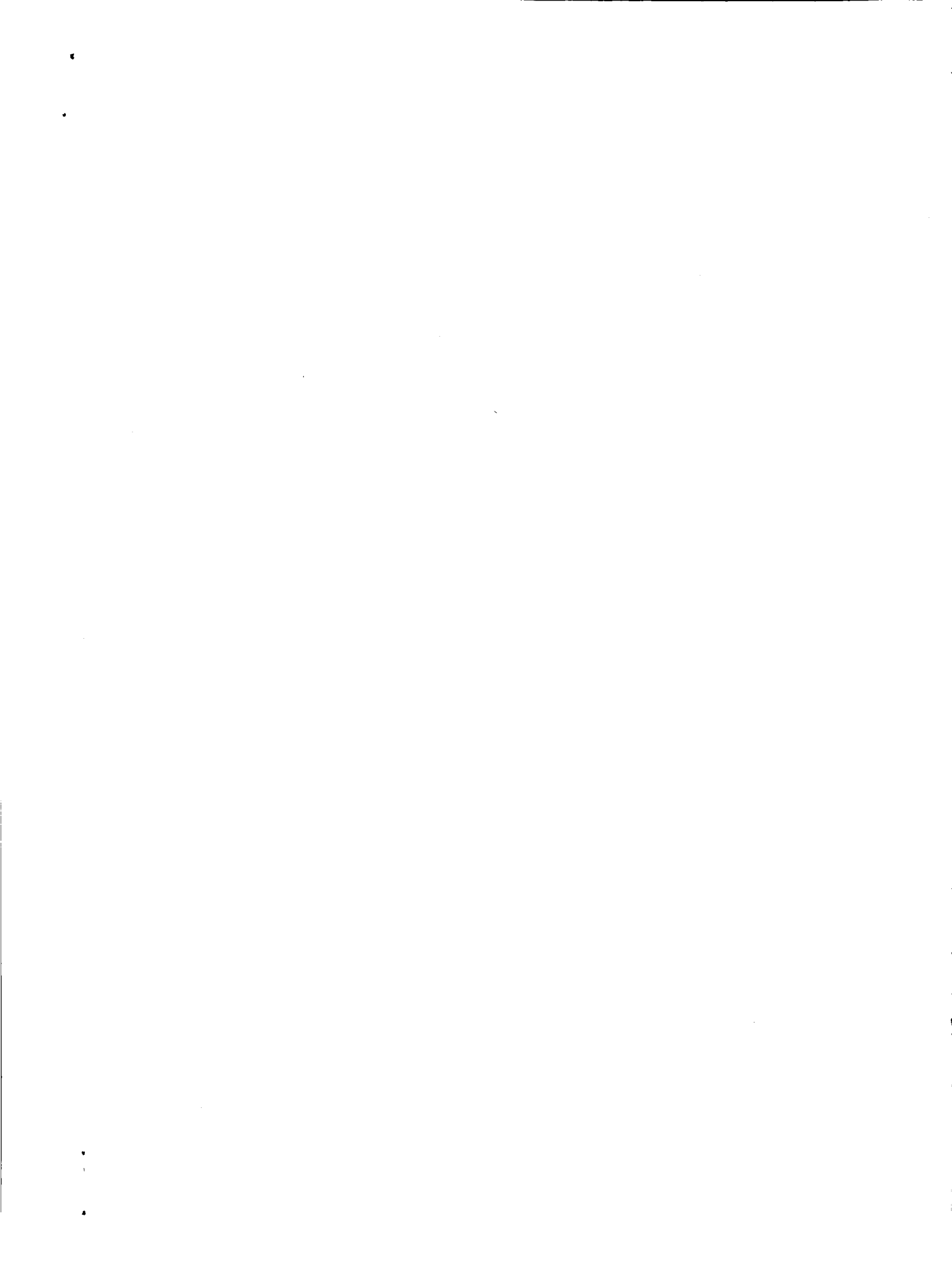
Distribution of this report is provided in the interest of information exchange. Responsibility for the contents resides in the author or organization that prepared it.

Issued by Originator as Report No. F-910091-10

Prepared under Contract No. NASw-847 by  
UNITED AIRCRAFT CORPORATION  
East Hartford, Conn.

for

NATIONAL AERONAUTICS AND SPACE ADMINISTRATION



## FOREWORD

An exploratory experimental and theoretical investigation of gaseous nuclear rocket technology is being conducted by the United Aircraft Corporation Research Laboratories under Contract NASw-847 with the joint AEC-NASA Space Nuclear Propulsion Office. The Technical Supervisor of the Contract for NASA is Captain W. A. Yingling (USAF). Results of the fluid mechanics portion of the investigation conducted during the period between September 15, 1965 and May 30, 1967 are described in the following four reports (including the present report) which comprise the required fifth Interim Summary Technical Report under the Contract:

1. Travers, A.: Experimental Investigation of Flow Patterns in Radial-Outflow Vortexes Using a Rotating-Peripheral-Wall Water Vortex Tube. UAC Research Laboratories Report F-910091-10, May 1967 (present report, NASA CR-991, 1968).
2. Johnson, B. V.: Exploratory Flow and Containment Experiments in a Directed-Wall-Jet Vortex Tube with Radial Outflow and Moderate Superimposed Axial Flows. UAC Research Laboratories Report F-910091-11, May 1967 (NASA CR-992, 1968).
3. Kendall, J. S., A. E. Mensing, and B. V. Johnson: Containment Experiments in Vortex Tubes with Radial Outflow and Large Superimposed Axial Flows. UAC Research Laboratories Report F-910091-12, May 1967 (NASA CR-993, 1968).
4. Clark, J. W., B. V. Johnson, J. S. Kendall, A. E. Mensing, and A. Travers: Summary of Gaseous Nuclear Rocket Fluid Mechanics Research Conducted Under Contract NASw-847. UAC Research Laboratories Report F-910091-13, May 1967. (Submitted to AIAA for publication.)



Experimental Investigation of Flow Patterns  
in Radial-Outflow Vortexes Using a Rotating-  
Peripheral-Wall Water Vortex Tube

TABLE OF CONTENTS

	<u>Page</u>
SUMMARY . . . . .	1
RESULTS AND CONCLUSIONS . . . . .	3
Basic Vortex Configuration . . . . .	3
Axial-Flow Vortex Configuration . . . . .	4
INTRODUCTION . . . . .	5
Background and Objectives of This Investigation . . . . .	6
DESCRIPTION OF EQUIPMENT AND PROCEDURES . . . . .	8
Description of Test Equipment . . . . .	8
Description of Test and Data Reduction Procedures . . . . .	10
REVIEW OF THEORETICAL CONSIDERATIONS FOR RADIAL-OUTFLOW VORTEXES . . . . .	12
Tangential Velocity Profiles . . . . .	12
Stability Criteria . . . . .	12
DISCUSSION OF RESULTS . . . . .	14
Results for Basic Vortex Configuration . . . . .	14
Results for Axial-Flow Vortex Configuration . . . . .	20
REFERENCES . . . . .	23
LIST OF SYMBOLS . . . . .	25
APPENDIX - RESULTS OF RADIAL-OUTFLOW TESTS IN THE 2144-PORT-INJECTION VORTEX TUBE . . . . .	27
TABLES . . . . .	29
FIGURES . . . . .	33

Experimental Investigation of Flow Patterns  
in Radial-Outflow Vortexes Using a Rotating-  
Peripheral-Wall Water Vortex Tube

SUMMARY

Experiments were conducted using a water vortex to investigate the conditions under which turbulence exists in radial-outflow vortexes with and without superimposed axial flow. The vortex test apparatus used had a 10-in.-dia by 30-in.-long rotating porous peripheral wall, a 1.0-in.-dia rotating inner porous tube located on the centerline, and end walls that could be rotated with the peripheral wall or held stationary. In the tests without superimposed axial flow (basic vortex configuration), plain end walls were used. Flow was injected through the inner porous tube, flowed radially outward, and was withdrawn through the rotating porous peripheral wall. In the tests with superimposed axial flow (axial-flow vortex configuration), one plain end wall and one end wall with a 3/4-in.-wide annulus near its outer edge were used. Flow was withdrawn through the annulus and was injected either (1) only through the inner porous tube, (2) through both the inner porous tube and the rotating porous peripheral wall, or (3) only through the rotating porous peripheral wall.

The characteristics of the flow were determined from observations and micro-flash photographs of dye patterns for different combinations of the flow conditions (values of tangential, radial and axial-flow Reynolds numbers) and the peripheral-wall, inner-porous-tube and end-wall rotation speeds. Tangential velocity profiles were measured for some basic-vortex flow conditions by means of a photographic particle-trace method using small, neutrally buoyant polystyrene spheres. Summary plots indicating criteria for the flow conditions that lead to laminar, alternating laminar and turbulent, and turbulent flow patterns were constructed for both vortex configurations.

The results of the tests indicate that radial-outflow vortexes are generally characterized by turbulence with large eddies that convect fluid from the central region of the vortex to near the peripheral wall. These flow patterns exist for both basic and axial-flow vortex configurations and for wide ranges of the flow conditions. Laminar flow was encountered only with low rates of radial outflow and low superimposed axial velocities. Rotation of the end walls had a significant effect on the flow patterns in the basic vortex configuration for a limited range of the flow conditions; rotation of the inner porous tube had no significant

effect. Rotation of the inner porous tube and end walls had no significant effect on the flow patterns in the axial-flow vortex configuration.

## RESULTS AND CONCLUSIONS

### Basic Vortex Configuration

- (1) With stationary end walls and no fluid injection through the stationary inner porous tube (radial Reynolds number,  $Re_r = 0$ ), the flow in the rotating-peripheral-wall vortex tube was laminar at all radii.
- (2) For the same configuration as (1) (stationary end walls and stationary inner porous tube) but with fluid injection through the porous tube (e.g.,  $Re_r = -30^*$ ), the flow was laminar from the centerline to a radius of approximately  $r = 2.5$  to  $3.5$  in. and was turbulent at larger radii. The radial extent of the laminar flow depended upon  $Re_r$  and the tangential Reynolds number,  $Re_{t,0}$ .
- (3) For the same configuration as (1) and (2) (stationary end walls and stationary inner porous tube) but in a jet-driven vortex tube (nonrotating peripheral wall), the flow was previously observed to be turbulent at all radii, indicating that jet injection has a detrimental effect on the entire flow field.
- (4) For the configuration of (2) but with the end walls rotating with the peripheral wall instead of stationary, the flow was laminar at all radii for small amounts of outflow ( $Re_r > -37$ ) at tangential Reynolds numbers up to  $Re_{t,0} = 300,000$ . For larger amounts of outflow and/or larger tangential Reynolds numbers (values of  $Re_r$  to  $-110$  and  $Re_{t,0}$  to  $330,000$  were investigated), the flow was at least partly turbulent. Within a small range of flow conditions, the flow oscillated between laminar and turbulent. Thus, the beneficial effects of end-wall rotation on radial-outflow flow patterns in basic vortex configurations are limited to flow conditions with small amounts of radial outflow.
- (5) For the configuration of (2) but with the inner porous tube rotating instead of stationary, the flow was completely turbulent for all ratios of peripheral-wall speed to inner-porous-tube speed. With inner porous tube and end walls rotating, the turbulence was decreased but could not be eliminated by very large peripheral-wall speeds.

---

\* Negative values of  $Re_r$  indicate radial outflow; the more negative  $Re_r$ , the larger the amount of radial outflow.

### Axial-Flow Vortex Configuration

- (1) The axial-flow Reynolds number,  $Re_{z,w}$ , and the ratio of average axial velocity in the vortex to the velocity of the rotating peripheral wall,  $\bar{V}_{z,w}/V_{\phi,0}$ , were observed to be the two major parameters which affected the flow patterns. For radial outflows, the radial Reynolds number,  $Re_r$ , and the condition of the end walls and the inner porous tube (i.e., whether stationary or rotating) had very little effect on the flow patterns.
- (2) For values of  $Re_{z,w}$  less than 3,000 and  $\bar{V}_{z,w}/V_{\phi,0}$  less than 0.01, (i.e., for small amounts of axial flow), the flow was laminar from the centerline to a radius of approximately  $r = 2.5$  in. and was turbulent at larger radii.
- (3) For values of  $Re_{z,w}$  and  $\bar{V}_{z,w}/V_{\phi,0}$  greater than in (2) above (values up to 21,000 and 0.3, respectively, were investigated), the flow was turbulent at all radii. Thus, the flow in the central region of a radial-outflow, axial-flow vortex is laminar only for small amounts of axial flow.
- (4) The turbulent flow observed for values of  $Re_{z,w}$  greater than 3,000 and  $\bar{V}_{z,w}/V_{\phi,0}$  greater than 0.01 was characterized by large eddies (approximately the size of half the radius of the vortex tube) in both the azimuthal ( $r-\phi$ ) and axial ( $r-z$ ) planes. These eddies convect fluid rapidly from the central region of the vortex to near the peripheral wall.
- (5) A limited number of tests of radial-inflow vortices with axial flow (vortices in which a portion of the flow is removed through the thru-flow ports at the centers of the end walls) were also conducted in the rotating-peripheral-wall vortex test apparatus. Laminar flow was observed in the central region, even at large values of  $Re_{z,w}$  and  $\bar{V}_{z,w}/V_{\phi,0}$  where radial-outflow vortices were observed to be turbulent.

## INTRODUCTION

An experimental and theoretical investigation of gaseous nuclear rocket technology is being conducted by the United Aircraft Research Laboratories under Contract NASw-847 administered by the joint AEC-NASA Space Nuclear Propulsion Office. The research performed under this contract is applicable to two vortex-stabilized gaseous nuclear rocket concepts: the open-cycle engine concept and the nuclear light bulb concept.

In the open-cycle concept, hydrogen propellant is injected from the peripheral wall of the rocket chamber to drive the vortex. It then flows axially in a narrow region near the peripheral wall into an exhaust annulus at one end of the chamber and through the exhaust nozzle. Gaseous nuclear fuel is contained in the central region of the vortex flow. Heat is transferred by thermal radiation from the gaseous nuclear fuel to the hydrogen propellant passing over the fuel region. Details of the engine concept -- including the fluid mechanics, heat transfer, nucleonics and structure -- are described in Ref. 1.

In the nuclear light bulb concept, propellant is heated by thermal radiation passing through an internally cooled transparent wall located between the fuel and the propellant. Coolant gas to drive a vortex is injected tangent to the inner surface of the transparent peripheral wall. In the nuclear light bulb, a vortex flow pattern is utilized to contain gaseous nuclear fuel and keep it away from the transparent wall.

Two factors which determine the flow patterns in confined vortexes are (1) whether or not there is a superimposed axial flow near the peripheral wall, and (2) whether or not the net flow of fluid is radially inward or outward with respect to the centerline of the vortex. In a vortex with superimposed axial flow, fluid is injected at the peripheral wall and is withdrawn through an annulus located near the outer edge of one end wall. The radial-inflow vortex is formed by removing a small amount of fluid through ports at the centers of the end walls. The radial-outflow vortex also is formed by injecting fluid at the peripheral wall, but in this case some fluid is also injected through the ports at the centers of the end walls.

Flow visualization tests of radial-inflow vortexes (Refs. 2 and 3) have indicated that the flow in the central region can be relatively laminar and, hence, may lead to satisfactory containment of gaseous nuclear fuel. However, two-component-gas tests with radial-inflow vortexes (Refs. 4, 5, and 6) have indicated that the density of the heavy gas in the simulated fuel-containment region of the vortex (i.e., the relatively laminar central region) can be only slightly greater than that of the surrounding light gas before instabilities and turbulence occur. In an open-cycle engine the density of the fuel must be considerably greater than that of the surrounding propellant; performance studies indicate that the fuel-to-propellant

density ratios attainable with a radial-inflow vortex are not large enough for such an engine. However, since the nuclear light bulb engine could utilize a heavy gas such as neon between the fuel and the transparent wall, radial-inflow vortices appear suitable for nuclear light bulb engines.

Initial flow visualization tests of radial-outflow vortices (Ref. 2) indicated that the flow was turbulent in the central region. However, two-component-gas tests (Refs. 5 and 6) indicated that the density of the heavy gas in the simulated fuel-containment region could be increased to a value substantially greater than the density of the surrounding light gas. However, very few measurements have been made of heavy-gas loss rates, particularly for conditions with large amounts of superimposed axial flow. Thus, further research was required to determine whether radial-outflow vortices would be suitable for application to an open-cycle engine.

Three different experimental investigations were conducted concurrently to investigate the characteristics of radial-outflow vortices for potential application to an open-cycle engine. The results of flow visualization tests directed toward obtaining fundamental information on flow stability and flow patterns in radial-outflow vortices are presented in this report. The results of an exploratory investigation that included flow visualization tests, flow-field velocity measurements and heavy-gas containment tests are reported in Ref. 7. The results of heavy-gas containment tests conducted at Reynolds numbers up to those that would be required in a full-scale engine are reported in Ref. 8. A summary of the principal results of the fluid mechanics research conducted under Contract NASw-847 and a comparison of the observed flow characteristics with those that would be required in both an open-cycle engine and a nuclear light bulb engine are presented in Ref. 9.

### Background and Objectives of This Investigation

Previous tests of radial-outflow water vortices driven by fluid injection through slots and jets in a stationary peripheral wall have indicated the existence of substantial amounts of turbulence (Ref. 2). Two possible sources of this turbulence were recognized: (1) mixing caused by the high-momentum fluid injected at the peripheral wall, and (2) an instability that might be inherent with the flow of fluid radially outward from the centerline of the vortex. To eliminate the first of these two possible sources, a rotating-peripheral-wall water-vortex apparatus was constructed in which the fluid enters or leaves at very low velocities relative to the moving wall of the vortex tube (and hence with low turbulence) through a large number of small holes drilled normally through the peripheral wall. Two other features, a rotating inner porous tube and end walls that can be rotated or held stationary, were also included in the new apparatus to permit investigation of the effects of these factors on the flow patterns. Both basic vortices (no axial flow) and vortices with superimposed axial flow can be investigated with this apparatus.

The objectives of the investigation reported herein were (1) to determine whether the turbulence that is observed in radial-outflow vortexes is caused by fluid injection at the peripheral wall or by an instability inherent with the flow of fluid radially outward from the centerline of the vortex, (2) to develop criteria for the flow conditions that lead to turbulence, and (3) to determine whether a rotating peripheral wall, a rotating inner porous tube, and rotating end walls have significant effects on the flow patterns.

## DESCRIPTION OF EQUIPMENT AND PROCEDURES

### Description of Test Equipment

#### Vortex Tube

The transparent-wall water vortex apparatus used in this investigation had a rotating peripheral wall, a rotating inner porous tube, and end walls that could be rotated with the peripheral wall or held stationary. A photograph of the apparatus is shown in Fig. 1. The vortex was contained within a 10-in.-ID by 30-in.-long rotating lucite cylinder (the peripheral wall) having 16,000 holes of 0.062-in.-dia drilled normally through the wall. This rotating peripheral wall (Fig. 1) was surrounded by a 14-in.-ID stationary lucite cylinder that formed a plenum for injecting or withdrawing water through the holes in the peripheral wall. The apparatus could be operated with or without a separately driven inner porous tube (not installed when the photograph in Fig. 1 was taken). The inner porous tube was fabricated from porous metal and had an OD of 1.0 in. The peripheral wall was driven by a 3/4-hp d-c motor with a variable-speed controller which regulated rotational speed to  $\pm 1$  percent from 40 to 456 rpm. The inner porous tube was driven by a 1/4-hp d-c motor with a similar variable-speed controller that provided regulation to within  $\pm 1$  percent from 100 to 2400 rpm. The end-wall drive spool (see Fig. 1) could be locked to the peripheral-wall drive or to the test stand. This allowed the end wall to be rotated with the peripheral wall or held stationary.

Experiments were conducted using vortex tube configurations with and without superimposed axial flow. Details of the configurations investigated are shown in Fig. 2 and sketches of the fluid injection methods used are shown in Fig. 3. In tests without superimposed axial flow (the basic vortex configuration, Fig. 2a) plain lucite end walls were used. Fluid was injected into the vortex tube through ports at the centers of the end walls or through the 1-in.-dia inner porous tube; fluid was withdrawn through the rotating porous peripheral wall (Fig. 3a). In tests with superimposed axial flow (the axial-flow vortex configuration, Fig. 2b) one plain lucite end wall and one lucite end wall with a 3/4-in.-wide annulus near its outer edge were used. Flow was withdrawn through the annulus at the axial-flow end wall and was injected either (1) only through the inner porous tube, (2) only through the rotating porous peripheral wall, or (3) through both the inner porous tube and the rotating porous peripheral wall (Fig. 3b).

Tests were also conducted using the 2144-port-injection vortex tube of Ref. 2 (a jet-driven vortex) with additional fluid injection through an inner porous tube. The results of these tests are discussed in the Appendix. This vortex tube had a stationary peripheral wall with 2144 injection ports of 0.060-in. dia; the inward injection angle for all ports was 19 deg measured with respect to the tangent at

the wall at the point of injection. A complete description of the 2144-port-injection vortex tube is given in Ref. 2.

### Flow Control System

In the basic vortex configuration, water was pumped from a storage tank through the inlet pipes leading to the ports in the end walls or to the inner porous tube. Measurements of the total flow injected into the vortex tube were made using rotameters located in the inlet pipes. In the axial-flow configuration, similar flow measurements were made for the flow injected through the porous tube. The flow injected through the rotating porous peripheral wall was measured using a turbine flow meter located in the inlet flow pipe leading to the injection plenum surrounding the rotating peripheral wall. The desired flow conditions were obtained by separate adjustment of control valves located upstream of the inner porous tube and peripheral-wall plenum. Measurements of water temperature were made using a thermometer located in the storage tank to determine the actual kinematic viscosity for calculating Reynolds numbers.

### Optical System and Flow Visualization Techniques

Flow visualization was provided by injection of fluorescent dye into the vortex through the inner porous tube or through the thru-flow ports at the centers of both end walls. A sketch of the optical system used to photograph dye patterns is shown in Fig. 4 (the chopping wheel was not used). Photographs of dye patterns were taken through an end wall of the vortex tube with illumination through an adjustable slit (usually 1/4 in. wide). Time exposure photographs of the dye patterns were also taken through the side wall of the vortex tube by interchanging the locations of the camera and light source. A microflash lamp having 0.1-microsecond flash period was used as the light source for photographs of the dye patterns taken through the end wall. The mercury vapor lamp used as the light source for the photographs taken through the side wall was powered by a 1-kw d-c power supply.

Tangential velocities in the primary-flow region of the vortex were measured for some flow conditions. The velocities were determined from time-exposure photographs of neutrally buoyant polystyrene spheres injected into the flow through a special port located on the inner porous tube near one end wall. The optical system shown in Fig. 4 was used to photograph the particles. The chopping disc contained 20 or 40 slots, depending on the flashing rate desired, and was driven by a variable-speed d-c shunt motor which allowed the flashing rate to be varied from 60 to 3000 flashes per sec. Intermittent illumination of the suspended particles caused them to appear as a series of streaks on a time exposure (see typical particle-trace photograph in Fig. 5). This technique permitted quantitative evaluation of the tangential velocities within the confined vortex without using probes which would tend to disturb the flow.

To select test particles, small quantities of expandable polystyrene spheres were heated and then dispersed in water. Those which remained suspended after 30 minutes were drawn off, dried and sized. Particles selected in this manner were almost neutrally buoyant. The particles used in these tests ranged in diameter from 0.033 to 0.078 in.

## Description of Test and Data Reduction Procedures

### Range of Flow Conditions Investigated

A summary of the combinations of geometric and flow parameters that were investigated using the basic vortex configuration is presented in Table I. The geometric parameters varied were the end-wall configuration (i.e., whether held stationary or rotated with the same speed as the peripheral wall) and inner porous tube configuration (stationary or rotating). The flow parameters varied were the tangential and radial Reynolds numbers. The tangential Reynolds number is defined as

$$Re_{t,o} = \frac{\pi N_o r_o^2}{30 \nu} \quad (1)$$

where  $N_o$  is the peripheral-wall speed in rpm and  $\nu$  is the kinematic viscosity for the water temperature at the time the tests were conducted. Peripheral-wall speed was varied from  $N_o = 40$  to 250 rpm in the tests; the corresponding tangential Reynolds numbers were from  $Re_{t,o} = 67,000$  to 410,000. The radial Reynolds number is defined as

$$Re_r = \frac{Q_f}{2 \pi \nu L} \quad (2)$$

where  $Q_f$  is the total volume flow rate of fluid injected through the ports at the centers of the end walls or through the inner porous tube. Using the sign convention adopted, when the net flow is radially outward in the primary flow (for most of the tests described herein),  $Re_r$  is negative. For these cases, the more negative  $Re_r$  the greater the amount of fluid flowing radially outward. Radial Reynolds numbers from 0 to -105 were investigated in the basic vortex configuration. When the net flow is radially inward (in some tests of the axial-flow vortex configuration, flow was withdrawn through the ports at the centers of the end walls),  $Re_r$  is positive.

A summary of the flow conditions that were investigated using the axial-flow vortex configuration is presented in Table II. This table is divided into four

sections, each listing the combinations of geometric and flow parameters investigated for the respective fluid injection methods. The same geometric parameters were varied as in the basic vortex configuration. Peripheral-wall speed was varied from  $N_0 = 40$  to 240 rpm; the corresponding tangential Reynolds numbers were from  $Re_{t,0} = 67,000$  to 394,000. Radial Reynolds number was varied from +90 (radial inflow) to -150 (radial outflow). Two other flow parameters, the axial-flow Reynolds number,  $Re_{z,w}$ , and the ratio of the average axial velocity in the vortex tube to the tangential velocity of the peripheral wall,  $\bar{V}_{z,w}/V_{\phi,0}$ , were also varied. The axial-flow Reynolds number is defined as

$$Re_{z,w} = \frac{Q_z}{(7/16)\pi r_0 \nu} \quad (3)$$

Values of  $Re_{z,w}$  from 880 to 21,000 and  $\bar{V}_{z,w}/V_{\phi,0}$  from 0.003 to 0.313 were investigated.

#### Reduction of Particle-Trace Data

The first step in the procedure for obtaining local tangential velocities in the primary-flow region was to determine the radius of a particle-trace from a photograph (see Fig. 5). Two points at the ends of dashes were selected and the circumferential distance between them was calculated from the radius and the central angle subtended. The time of travel was determined from the number of dashes between the points and the light flashing rate. The tangential velocity was then calculated by dividing the circumferential distance by the time of travel. The photographs from which the tangential velocities were determined were taken with light illumination at the axial mid-plane for all profiles presented in this report.

## Tangential Velocity Profiles

Theoretical radial-outflow tangential velocity profiles for rotating flows without superimposed axial flow are shown in Fig. 6. This figure will aid in interpreting differences in tangential velocity profiles measured in the basic vortex configuration. The profiles were calculated for a velocity distribution of the form

$$v_{\phi} \propto r^{(n_{\Gamma} - 1)} \quad (4)$$

Profiles of this form are solutions to the Navier-Stokes equations for laminar radial outflow in which the local radial Reynolds number ( $Re_{r,p} = v_r r / \nu$ ) and viscosity are assumed independent of radius. According to theory,

$$n_{\Gamma} = 2 - Re_{r,p} \quad (5)$$

Calculations were made for various values of  $Re_{r,p}$  (Fig. 6) to simulate certain measured tangential velocity profiles (see following section).

The effect of the ratio of total-to-laminar viscosity ( $\rho\epsilon/\mu$ , an indication of turbulence level) may be noted in Fig. 6. For a constant value of  $Re_{r,p}$ , the effect of increasing turbulence (increasing  $\rho\epsilon/\mu$ ) is to drive the profile towards solid-body rotation (towards  $v_{\phi} \propto r$ , the profile for  $Re_{r,p}/(\rho\epsilon/\mu) = 0$ ). Turbulence reduces the effective outflow radial Reynolds number and increases the tangential velocities in the central region of the vortex. It is known from observations of the flow patterns that  $Re_{r,p}$  and  $\rho\epsilon/\mu$  are not constant with radius; therefore, the information in Fig. 6 is only useful to help explain general trends.

## Stability Criteria

There is no existing single theoretical stability criterion that covers all of the possible disturbances which might lead to instabilities in the types of flows considered in this investigation. Although a large body of literature exists on the stability of rotating flows, a major part treats only axisymmetric disturbances of the type identified by Lord Rayleigh. Only recently have there been studies which considered the effects of axial velocity gradients in the flow and

nonaxisymmetric disturbances. Results of analyses of the stability of inviscid flows in the annulus between two closely spaced concentric rotating cylinders are given in Refs. 10 through 12. Disturbances of arbitrary asymmetry are allowed, including disturbances in both the azimuthal and axial directions. References 10 and 11 consider the special case of a constant-density flow with linear tangential and axial velocity profiles in the annulus, i.e., with constant tangential and axial velocity gradients. The local slope of the tangential velocity profile given by Eq. (4) can be related to the linear profiles of Refs. 10 and 11. According to the theory of Refs. 10 and 11, the flow will be stable for values of  $n_T > 2.667$  for all axial velocity gradients.

An extension of the basic Rayleigh criterion to flow with radial density gradients is given in Ref. 13 but, like the Rayleigh criterion, the criterion is valid only for axisymmetric disturbances. The criteria of Refs. 10 and 11 have been extended to cover the case of linear radial gradients of density in Ref. 12. The results of Ref. 12 are in agreement with the results of Refs. 10 and 11 in the limit of constant density. The criterion of Ref. 12 predicts stability for all disturbances including tangential shear modes in constant-density radial outflows with linear tangential velocity profiles and no axial velocities. Shear instabilities are encountered in parallel flow when there is an inflection in the velocity profile. The corresponding criterion for tangential shear instabilities in rotating flow is an inflection in vorticity (Refs. 14 and 15).

The results obtained in Refs. 10 through 12 appear to represent the most applicable stability criteria for gaseous nuclear rockets available at the present time. These criteria are clearly not adequate, however, because (1) they do not treat the general case of arbitrary tangential and axial velocity profiles, and (2) they do not include the influence of viscosity. It is not likely that significant improvements in these criteria can be made in the near future due to the complexity of the problem. Therefore, the results of experiments such as those discussed in this report must be relied on for empirical knowledge of the stability of rotating flows.

## DISCUSSION OF RESULTS

### Results for Basic Vortex Configuration

Sketches of the two fluid injection methods which were used with radial-outflow vortexes without superimposed axial flow are shown in Fig. 3a. A summary of the flow conditions investigated is presented in Table I.

#### Effect of Vortex Driving Method

Microflash photographs showing typical flow patterns in the rotating-peripheral-wall vortex tube and 2144-port-injection vortex tube (the latter from the tests reported in Ref. 2) are shown in Fig. 7. These and all other photographs in this report that were taken through an end wall show flow patterns at the axial mid-plane. In all photographs, the flow is rotating counterclockwise as indicated by the arrow. It is sometimes difficult to determine whether the flow is laminar or turbulent from photographs of dye patterns. For radial inflow vortexes (e.g., Ref. 2) it is clear from the appearance of fine dye that the flow is laminar. In radial-outflow vortexes, large turbulent eddies are often visible. For other cases where the photographs show slightly irregular or diffuse dye patterns, observations from a series of tests are needed to determine whether the flow is laminar or turbulent.

The effect of the vortex driving method on the flow patterns can be observed by comparing the flow patterns in Fig. 7a with those in Fig. 7b. For these tests the end walls of both vortex tubes were stationary. The upper photographs in Figs. 7a and 7b show the flow patterns without fluid injection through an inner porous tube (the inner porous tube was not installed), i.e., for  $Re_p = 0$ . In the rotating-peripheral-wall vortex tube, where the vortex is driven by the rotating wall, the flow was laminar at all radii as shown by the fine spiral dye filaments (upper photograph of Fig. 7a). In the 2144-port-injection vortex tube, where the vortex is driven by fluid injected through the fixed ports, the flow was turbulent at all radii as shown by the diffuse dye pattern with small eddies (upper photograph of Fig. 7b). The lower photographs in Figs. 7a and 7b show the flow patterns with fluid injection through a stationary inner porous tube. In the rotating-peripheral-wall vortex tube (lower photograph of Fig. 7a), the flow was laminar from the centerline to a radius of about 2.5 in. as shown by the stratified structure of the dye pattern. The noncircular appearance of the dye filaments is due to slightly nonuniform fluid injection through the inner porous tube. At radii greater than 2.5 in., the flow was turbulent as indicated by the dye filaments breaking up into eddies. In the 2144-port-injection vortex tube (lower photograph of Fig. 7b), the flow was turbulent at all radii. Thus the flow was partly or completely laminar in the rotating-peripheral-wall vortex tube with and without fluid injection through the inner porous tube while the flow was completely

turbulent in the 2144-port-injection vortex tube. This indicates that the vortex driving method is important and that jet injection has a detrimental effect on the entire flow field.

For all cases tested in the rotating-peripheral-wall vortex tube with stationary end walls and fluid injection through the stationary inner porous tube, the flow was laminar from the centerline to a radius of approximately  $r = 2.5$  to  $3.5$  in. and was turbulent at larger radii (i.e., flow patterns like the one in the lower photograph of Fig. 7a). The radial extent of the laminar flow depended upon the radial and tangential Reynolds numbers. With no net outflow ( $Re_r = 0$ ; upper photograph of Fig. 7a), the flow was laminar at all radii. Although  $Re_r = 0$  indicates no net outflow, there is usually local radial inflow in the end-wall boundary layers and corresponding local radial outflow in the primary-flow region. The presence of local radial outflow at the axial mid-plane can be inferred from the spiral nature of the dye pattern in Fig. 7a and from a comparison of the measured tangential velocity profile for  $Re_r = 0$  in the rotating-peripheral-wall vortex tube (Fig. 8) with the theoretical profiles in Fig. 6. Assuming that  $\rho\epsilon/\mu = 1$  (a valid assumption since the flow patterns were laminar), the measured profile for  $Re_r = 0$  is very similar to the theoretical profile for  $Re_{r,p} = -6$ ; therefore, a small radial outflow existed in the primary flow. The fluid which is being driven by the rotating-peripheral-wall flows axially into the end-wall boundary layers at large radii, flows radially inward in the end-wall boundary layers, flows axially out into the primary flow at small radii, and again flows radially outward in the primary flow. Thus the above results indicate that local radial outflows are laminar for very small outflows; however, they are inherently unstable (most likely a tangential shear mode instability) with any significant net radial outflow.

The effect of the vortex driving method on the measured tangential velocity profiles is shown in Fig. 8. In general, no large differences are observed in the shape of these profiles; they are all basically the type encountered in radial-outflow vortices. However, the small differences in the profiles for a given radial Reynolds number in the two vortex tube configurations can be explained with the aid of the theoretical profiles in Fig. 6. It will be noted in Fig. 6 that an increase in turbulence for any constant value of  $Re_{r,p}$  tends to drive the tangential velocity profile toward solid-body rotation, i.e., toward  $v_\phi \propto r$ . The effect of turbulence is to reduce the effective outflow radial Reynolds number of the flow which increases the tangential velocities in the central region of the vortex. It will be noted in Fig. 8 that, for the same value of  $Re_r$ , the measured tangential velocity profile in the 2144-port-injection vortex tube (in which the flow was turbulent) is closer to solid-body rotation than the corresponding profile in the rotating-peripheral-wall vortex tube (in which the flow was laminar).

As noted in the preceding section, criterion for tangential shear instability in rotating flows is an inflection in the vorticity. The tangential profiles shown

in Fig. 8 do not have either an inflection in the velocity or an inflection in vorticity and, therefore, should be stable by the above criterion. However, it should be noted that this criterion is only valid for two-dimensional inviscid flows without consideration of the axial velocities induced by secondary-flow effects.

#### Effect of Fluid Injection Method

Tests were conducted with fluid injection through the thru-flow ports located at the centers of the end walls in order to compare this injection method with fluid injection through the inner porous tube. Sketches of these fluid injection methods are shown in Fig. 3a. Typical flow patterns for fluid injection through the thru-flow ports and through the stationary inner porous tube are shown in Fig. 9 for both stationary and rotating end walls. For fluid injection through the thru-flow ports, the flow was very turbulent with both stationary and rotating end walls. The flow with fluid injection through the inner porous tube was laminar as indicated by the stratified structure of the dye patterns in the upper and lower photographs of Fig. 9b. Thus, all further tests were conducted with fluid injection through the inner porous tube.

#### Effect of End-Wall Rotation

As discussed previously, the flow patterns with fluid injection through the stationary inner porous tube and with stationary end walls were laminar from the porous tube to a radius of approximately 2.5 to 3.5 in. and were turbulent at larger radii. Typical flow patterns for these conditions are shown in Fig. 10a. The upper photograph was taken approximately 25 sec after dye injection and the lower photograph was taken approximately 50 sec after dye injection. The fluid moved radially outward from the porous tube through the laminar region, past a radius of about 2.5 in., and into a region of flow containing high-angular-momentum fluid where the tangential velocities varied from about 0.1 ft/sec at a radius of 3.5 in. to 3 ft/sec at the peripheral wall (see the measured velocity profiles in Fig. 11). Because the fluid injected through the inner porous tube had no angular momentum, turbulent shear occurred in this outer region as indicated in the lower photograph of Fig. 10a. This situation would lead to the tangential shear instability previously mentioned.

For the same fluid injection method, but with the end walls rotating with the peripheral wall, the flow was laminar at all radii for moderate amounts of radial outflow ( $Re_r$  from 0 to -37). Typical flow patterns for these conditions are shown in Fig. 10b. The flow moved radially outward from the porous tube as shown by the stratified laminar dye layers in the upper photograph of Fig. 10b to a radius of approximately 2.5 in.; then, most of the flow moved axially toward the end walls with the remaining flow moving very slowly radially outward as shown in the lower photograph of Fig. 10b.

Typical tangential velocity profiles for cases with stationary and rotating end walls at the same  $Re_r$  as the flow patterns shown in Fig. 10 are shown in Fig. 11. The shape of the profiles are similar; no inflections in the tangential velocity profiles that could be associated with possible turbulence-producing mechanisms are observable. The difference in the profiles can possibly be explained on the basis of a difference in the local radial Reynolds number. For the case with rotating end walls, most of the injected flow was pumped axially at small radii and entered the end-wall boundary layers; hence, the local radial outflow in the primary-flow region was small. For the case with stationary end walls, the injected flow moved radially outward at all radii except near the peripheral wall where some of the flow moved axially.

A summary of the laminar and turbulent flow conditions observed with rotating end walls and with fluid injection through the stationary inner porous tube is shown in Fig. 12. As indicated previously, flow patterns for small amounts of outflow ( $Re_r > -37$ ) were laminar at all radii for tangential Reynolds numbers up to about 300,000 (Fig. 12). At  $Re_{t,o} = 300,000$ , the flow became very unstable and oscillated between turbulent and laminar flow. This is a particularly interesting result because the transition Reynolds number for the flow on a disk rotating in an infinite medium is also approximately 300,000 (Ref. 16). At  $Re_r = -37$ , periodic transition to turbulent flow was observed (that is, the flow was alternately laminar and turbulent) in the boundary layer on the right end wall at a radius of about 3 in. This turbulence in turn caused portions of the primary flow to be alternately laminar and turbulent. The axial extent and the duration of the observed turbulence varied with the peripheral-wall rotational speed. For example, at a rotational speed of 40 rpm ( $Re_{t,o} = 67,000$ ), the axial extent of the turbulence was about 5 in. from the right end wall; the duration of the turbulent flow was about 50 sec and the duration of the laminar flow was about 90 sec. The remaining portions of the vortex flow, including the left end-wall boundary layer, remained laminar at all times. As rotational speed was increased, the axial extent and duration of turbulence was increased until the entire flow field became turbulent at  $Re_{t,o} = 280,000$ . At  $Re_r < -37$  (larger amounts of outflow), turbulence occurred continuously near the right end wall (see the "Partly Turbulent" region in Fig. 12). Its axial extent was a function of peripheral-wall rotational speed; the other portions of the flow remained laminar. Also, as the outflow was increased, the rotational speed at which the entire flow became turbulent decreased. An example of the above phenomenon is shown in the photographs in Fig. 13 for  $Re_r = -45$ . The upper photograph (taken through the front of the vortex tube) shows the dye trace for  $N_o = 73$  rpm. The turbulence extends approximately 13 in. axially from the right end wall. In the lower photograph, at  $N_o = 156$  rpm, the turbulence extends approximately 24 in. axially from the right end wall. It is not known why transition to turbulence always started at the right end wall.

A comparison of the measured tangential velocity profiles for two different radial Reynolds numbers leading to partly turbulent and completely laminar flow

patterns is shown in Fig. 14. The profile for partly turbulent flow ( $Re_r = -48$ ) corresponds to a flow pattern similar to the pattern shown in the upper photograph in Fig. 13. The profile for completely laminar flow ( $Re_r = -30$ ) corresponds to a flow pattern similar to that in Fig. 10b. The small difference in the profiles can be attributed to the difference in the amount of radial outflow for the two cases. However, again there are no observable inflection points or other significant differences in the profiles which could be associated with a driving mechanism for unstable or turbulent flows. In general, there is a lack of any distinguishing differences between the measured tangential profiles for laminar flow, partly turbulent flow and completely turbulent flow in Figs. 8, 11, and 14.

#### Typical Streamline Pattern

Figures 15 and 16 supply the information necessary to construct a sketch of the streamline pattern for a typical completely laminar flow condition. Figure 15 presents photographs of three dye patterns in the  $r$ - $z$  plane near the right end wall for  $Re_r = -15$  and  $Re_{t,0} = 117,000$ . These photographs were taken at various times after dye injection. The upper photograph in Fig. 15 shows fluid which has been injected through the stationary inner porous tube moving radially outward, moving axially toward the right end wall, entering the end-wall boundary layer, and again moving radially outward (see sketch in Fig. 17). The middle photograph shows the lower portion of a recirculation cell which has formed and, below that, a horizontal annular dye trace which moves radially outward with time. The photograph also shows the minimum radius of the recirculating flow which reenters the end-wall boundary layer (shown in Fig. 17); note in the photograph the indentation in the horizontal dye trace at the end wall. The lower photograph in Fig. 15 shows that the horizontal annular dye trace has moved outward to a larger radius and has joined the lower portion of the recirculation cell.

The variation of local radial Reynolds number with radius at the axial mid-plane for the same flow conditions is shown in Fig. 16. Photographs of the horizontal annular dye trace were taken at different times at the axial mid-plane. A curve of the radius of the dye trace vs time was constructed from the photographs and its slope was measured to determine local radial velocities and local radial Reynolds numbers. The curve in Fig. 16 correlates very well with the dye pattern photographs. The decrease in local radial Reynolds number in the primary flow between radii of 2 and 3.3 in. indicates that the flow is moving into the end-wall boundary layers. The flow in the end-wall boundary layers reaches a maximum at a radius of 3.3 in. (the minimum point of the curve). At this point,  $Re_{r,p} = 1.1$ ; this value of  $Re_{r,p}$  indicates that approximately 92.5 percent of the total injected flow was in the boundary layers. This radius compares closely with the minimum radius of the recirculating flow noted in the middle photograph in Fig. 15. At radii greater than 3.3 in., the remaining 7.5 percent of the flow and the flow which reenters the primary-flow region from the end-wall boundary layers continues to move radially outward (note the increase in outflow at large radii in Fig. 16).

A streamline pattern constructed from the above information is shown in Fig. 17. Note that a portion of the flow that enters the end-wall boundary layer flows into recirculation cells formed at both end walls. A possible explanation of this phenomenon can be described with the aid of Fig. 18. This figure shows the theoretical radial outflow (in terms of the radial Reynolds number) in the laminar boundary layer on a disk rotating in an infinite medium at several rotational speeds (relations obtained from Ref. 16). For  $N_0 = 110$  rpm, note that the total flow demanded by one end-wall boundary layer at  $r = 5.0$  is equivalent to  $Re_r = -31$ . However, in the experimental case for  $Re_r = -15$  (Figs. 15 through 17), assuming that the injected flow divides evenly, only flow equivalent to  $Re_r = -7.5$  is available for each end wall. Thus, to satisfy the flow requirements of the end-wall boundary layers, flow is recirculated into the end-wall boundary layers from the primary-flow region. This is the mechanism for formation of the recirculation cells in portions of the primary-flow region.

It was stated previously that the transition Reynolds number for flow on a disk rotating in an infinite medium was approximately  $Re_{t,0} = 300,000$ . The radial Reynolds number associated with this  $Re_{t,0}$  is  $Re_r = -40$  at  $r = 5.0$  in. (one end wall). It can be seen in Fig. 12 that for small radial outflows, transition to turbulence at  $Re_{t,0} = 300,000$  was observed. However, for large radial outflows ( $Re_r \leq -37$ , or  $\leq -18.5$  for one end wall), transition to turbulence occurred at the right end wall for very small values of  $Re_{t,0}$  (e.g.,  $Re_{t,0} = 67,000$  which was the lowest tested). One possible explanation for this premature transition to turbulence could be described on the basis of the flow in the corner between the peripheral wall and the end wall. For low radial outflows, the flow can negotiate this corner without separating and forming eddies; however, for large radial outflows, separation occurs in the corner causing transition to turbulence in the end-wall boundary layer. The adjacent portion of the primary-flow region also became turbulent because of the recirculation cell.

#### Effect of Rotating Inner Porous Tube

Tests were conducted to determine the effect of rotating the inner porous tube on the flow patterns. Tests were conducted with both stationary and rotating end walls with the inner porous tube and the peripheral wall rotating at low and high rotational rates. With stationary end walls, the flow was completely turbulent for all values of the ratio of peripheral-wall speed to inner-porous-tube speed,  $N_0/N_i$ . Typical flow patterns for these cases are shown in Figs. 19a and 20a. With the end walls rotating with the peripheral wall, the flow was turbulent for low values of  $N_0$  (less than 190 rpm) for all values of  $N_0/N_i$ ; the turbulence was decreased but not eliminated for values of  $N_0 > 190$  rpm and  $N_0/N_i < 0.3$ . Typical flow patterns for these cases are shown in Figs. 19b and 20b.

## Results for Axial-Flow Vortex Configuration

Tests of radial-outflow vortexes were conducted in the rotating-peripheral-wall vortex tube with superimposed axial flow using three different fluid injection methods. Sketches of these fluid injection methods are shown in Fig. 3b. A fourth method, not shown in Fig. 3b but discussed later, was used in tests of radial-inflow vortexes. Table II is a summary of the flow conditions investigated for the four different fluid injection methods.

The fraction of total flow injected through the peripheral wall for different combinations of the radial and axial-flow Reynolds numbers ( $Re_r$  and  $Re_{z,w}$ ) is shown in Fig. 21. The curves in this figure will enable the reader to determine the relative amounts of flow injected through the inner porous tube and the peripheral wall from the values of  $Re_r$  and  $Re_{z,w}$ . For fluid injection through the inner porous tube only, combinations of  $Re_r$  and  $Re_{z,w}$  will lie on the extreme left-hand curve in Fig. 21. For fluid injection through the peripheral wall only, combinations of  $Re_r$  and  $Re_{z,w}$  will lie along the abscissa. Combinations of  $Re_r$  and  $Re_{z,w}$  falling between the above limits indicate that fluid was injected through both the peripheral wall and inner porous tube in the fractions indicated. The ratio of the average axial velocity in the vortex tube to the peripheral-wall velocity,  $\bar{V}_{z,w}/V_{\phi,0}$ , is also a parameter in tests with axial flow.

### Effects of $Re_{z,w}$ and $\bar{V}_{z,w}/V_{\phi,0}$

----- Tests at  $Re_{z,w} < 3000$  and  $\bar{V}_{z,w}/V_{\phi,0} < 0.01$  -----

The results of tests conducted at values of  $Re_{z,w}$  less than 3000 and  $\bar{V}_{z,w}/V_{\phi,0}$  less than 0.01 indicated that end-wall configuration (whether stationary or rotating) and fluid injection method had little effect on the flow patterns. This result is in strong contrast to the results for the basic vortex configuration where end-wall configuration and fluid injection method had appreciable effects on the flow patterns. For these low values of  $Re_{z,w}$  and  $\bar{V}_{z,w}/V_{\phi,0}$  the flow patterns were laminar from the centerline to a radius of approximately 2.5 in. (the central region) and turbulent at larger radii (the outer region). Photographs of the dye patterns for cases with stationary and rotating end walls are shown in Fig. 22. The upper photographs in Figs. 22a and 22b show laminar flow in the central region (indicated by the stratified structure of the dye patterns). The noncircular appearance of the dye traces is due to slightly nonuniform fluid injection through the inner porous tube. The lower photographs in Fig. 22a and 22b both show turbulent flow in the outer flow region.

The effect of fluid injection method on the flow patterns at these low values of  $Re_{z,w}$  and  $\bar{V}_{z,w}/V_{\phi,0}$  can be seen by comparing the photographs in Figs. 22a, 23a, and 24a. In Fig. 22a, fluid was injected only through the inner porous tube; in Fig. 23a, fluid was injected only through the peripheral wall; and in Fig. 24a,

fluid was injected through both the peripheral wall and the inner porous tube. The flow was laminar in the central region (note the stratified structure of the dye traces) for all three injection methods. Although not shown in Figs. 23a and 24a, the flow was turbulent in the outer region.

Tests at  $Re_{z,w} > 3000$  and  $\bar{V}_{z,w} / V_{\phi,0} > 0.01$   
-----

For tests conducted at values of  $Re_{z,w}$  greater than 3000 and  $\bar{V}_{z,w} / V_{\phi,0}$  greater than 0.01 (values up to 22,000 and 0.3, respectively, were investigated), the results showed that end-wall configuration and fluid injection method had no effect on the flow patterns. The same result was obtained for tests with  $Re_{z,w}$  less than 3000 and  $\bar{V}_{z,w} / V_{\phi,0}$  less than 0.01. However, in contrast to the partly laminar flow patterns obtained in tests with  $Re_{z,w}$  less than 3000 and  $\bar{V}_{z,w} / V_{\phi,0}$  less than 0.01, all the flow patterns for  $Re_{z,w}$  greater than 3000 and  $\bar{V}_{z,w} / V_{\phi,0}$  greater than 0.01 were turbulent at all radii. These results indicate that  $Re_{z,w}$  and  $\bar{V}_{z,w} / V_{\phi,0}$  were the two major parameters which affected the flow patterns.

The effect of fluid injection method can be seen by comparing the photographs in Figs. 23b, 23c, and 24b. In Figs. 23b and 23c, fluid was injected only through the peripheral wall; in Fig. 24b, fluid was injected through both the peripheral wall and inner porous tube. The flows in all three photographs are turbulent with large-scale eddies. Similar size eddies were also noted in the  $r-z$  plane. The difference in the scale of the turbulence for flows at values of  $Re_{z,w}$  less than and greater than 3000 can be seen by comparing the above photographs with the lower photograph in Fig. 22a. For  $Re_{z,w} > 3000$ , eddies having diameters up to half the radius of the vortex tube were observed. These eddies convect fluid from the central region to the outer region of high axial velocities. For  $Re_{z,w} > 3000$ , eddies having diameters up to approximately 0.25 in. were observed.

#### Effect of Rotating Inner Porous Tube

No improvement in the flow characteristics was observed in tests conducted with the inner porous tube rotating at various speeds. Typical flow patterns at low and high axial-flow Reynolds numbers and with three different fluid injection methods are shown in Fig. 25. In all tests, the inner porous tube was rotating. The photographs show that the flow was turbulent at all radii in each case.

#### General Discussion of Test Results

The results of all tests conducted with radial outflow in the axial-flow vortex configuration with rotating and stationary end walls and with the inner porous tube stationary are summarized in Fig. 26. Flow conditions that were observed are indicated on a plot of  $\bar{V}_{z,w} / V_{\phi,0}$  vs  $Re_{z,w}$ . The ratio  $\bar{V}_{z,w} / V_{\phi,0}$  is equal to  $Re_{z,w} / Re_{t,0}$ ; lines of constant  $Re_{t,0}$  (corresponding to constant peripheral-wall rotational speed,  $N_0$ ) are also shown in Fig. 26. Flow conditions

observed to be laminar in the central region (from the centerline of the vortex to a radius of approximately 2.5 in.) are denoted by circle symbols; flow conditions observed to be turbulent in this region are denoted by triangle symbols; and flow conditions observed to alternately change from laminar to turbulent are denoted by cross symbols. This form of presentation does not show any differences in radial Reynolds number or end-wall conditions (i.e., whether stationary or rotating) because, as indicated previously, these factors were found to have very little effect on the flow patterns.

A possible boundary between the laminar and turbulent conditions has been drawn on Fig. 26. In the region of the boundary, most of the flow patterns were alternately laminar and turbulent. The unstable nature of the flow in this region was characterized by the onset of a periodic radial oscillation which resulted in the deformation of the initially laminar circular streamlines progressively into ellipses and then into large eddies. The laminar flow would then reappear and the break-up process would repeat. Dye photographs in Fig. 27 show this process before (Fig. 27a) and after (Fig. 27b) the onset of large eddies.

The principal results of these radial-outflow tests are that the flow was laminar in the central flow region only for small amounts of axial flow;  $Re_{z,w}$  less than 3000 and  $\bar{V}_{z,w} / V_{\phi,0}$  less than approximately 0.01. However, for values of  $Re_{z,w}$  greater than 3000 and  $\bar{V}_{z,w} / V_{\phi,0}$  greater than 0.01, the flow was turbulent at all radii and was characterized by large eddies. Thus, large superimposed axial flows and the associated axial shear only caused an already turbulent flow to deteriorate even further.

The shaded boundary in the upper right-hand corner of Fig. 26 encompasses combinations of  $\bar{V}_{z,w} / V_{\phi,0}$  and  $Re_{z,w}$  that were used in the two-component-gas vortex tests discussed in Refs. 7 and 8. The present results provide additional evidence that the poor containment characteristics of radial-outflow vortexes are caused by mixing of the heavy and light gases due to turbulence and large-scale eddies.

Several tests with superimposed axial flow but with radial inflow instead of radial outflow were also conducted. The inner porous tube was removed; flow was withdrawn through the axial-flow exhaust annulus and the thru-flow ports at the centers of the end walls. Two flow conditions having large values of  $Re_{z,w}$  and  $\bar{V}_{z,w} / V_{\phi,0}$  are indicated by the solid circle symbols in Fig. 26. For these and all other radial-inflow conditions that were investigated, the flow was laminar in the central region. A comparison of radial outflow and radial inflow patterns at large values of  $Re_{z,w}$  and  $\bar{V}_{z,w} / V_{\phi,0}$  is shown in Fig. 28.

## REFERENCES

1. McLafferty, G. H.: Analytical Study of the Performance Characteristics of Vortex-Stabilized Gaseous Nuclear Rocket Engines. United Aircraft Research Laboratories Report D-910093-20, prepared under Contract NASw-847, September 1965. To be issued as NASA CR report.
2. Travers, A.: Experimental Investigation of Peripheral-Wall Injection Techniques in a Water Vortex Tube. United Aircraft Research Laboratories Report D-910091-7, prepared under Contract NASw-847, September 1965. To be issued as NASA CR report.
3. Travers, A. and B. V. Johnson: Measurements of Flow Characteristics in an Axial-Flow Vortex Tube. United Aircraft Research Laboratories Report C-910091-3, prepared under Contract NASw-847, September 1964. Also issued as NASA CR-277.
4. Mensing, A. E. and J. S. Kendall: Experimental Investigation of Containment of a Heavy Gas in a Jet-Driven Light-Gas Vortex. United Aircraft Research Laboratories Report D-910091-4, prepared under Contract NASw-847, March 1965. To be issued as NASA CR report.
5. Mensing, A. E. and J. S. Kendall: Experimental Investigation of the Effect of Heavy-to-Light-Gas Density Ratio on Two-Component Vortex Tube Containment Characteristics. United Aircraft Research Laboratories Report D-910091-9, prepared under Contract NASw-847, September 1965. To be issued as NASA CR report.
6. Kendall, J. S. and A. E. Mensing: Experimental Investigation of the Effect of Heavy-to-Light-Gas Density Ratio on Vortex Containment Characteristics. United Aircraft Research Laboratories Report UAR-E54, prepared under Contract NASw-847, April 1966. Paper presented at AIAA Second Propulsion Joint Specialists Conference, Colorado Springs, Colo., June 13-17, 1966.
7. Johnson, B. V.: Exploratory Flow and Containment Experiments in a Directed-Wall-Jet Vortex Tube with Radial Outflow and Moderate Superimposed Axial Flows. United Aircraft Research Laboratories Report F-910091-11, prepared under Contract NASw-847, May 1967. To be issued as NASA CR report.
8. Kendall, J. S., A. E. Mensing and B. V. Johnson: Containment Experiments in Vortex Tubes with Radial Outflow and Large Superimposed Axial Flows. United Aircraft Research Laboratories Report F-910091-12, prepared under Contract NASw-847, May 1967. To be issued as NASA CR report.

9. Clark, J. W., B. V. Johnson, J. S. Kendall, A. E. Mensing, and A. Travers: Summary of Gaseous Nuclear Rocket Fluid Mechanics Research Conducted under Contract NASw-847. United Aircraft Research Laboratories Report F-910091-13, prepared under Contract NASw-847, May 1967. To be issued as NASA CR report.
10. Ludwig, H.: Stability of Flow in an Annular Space. Zeitschrift für Flugwissenschaften, Vol. 8, 1960, pp. 135-140.
11. Ludwig, H.: Extension of the Work on the Stability of Flow in an Annular Space. Zeitschrift für Flugwissenschaften, Vol. 9, 1961, pp. 359-361.
12. Kurzweg, U. H.: Criteria for the Stability of Heterogeneous Swirling Flows. United Aircraft Research Laboratories Report UAR-F96, May 1967.
13. Synge, J. L.: The Stability of Heterogeneous Liquids. Transactions of the Royal Society of Canada, Vol. 27, 1933, pp. 1-18.
14. Rayleigh, Lord: Scientific Papers I. Cambridge University Press, 1880, pp. 474-487.
15. Lary, E. C.: On the Shearing Instability of Rotating Flow. FOM-Instituut voor Plasma-Fysica (Rijnhuizen, Jutphaas, Nederland) Report WET 65/034, October 1965.
16. Schlichting, H.: Boundary Layer Theory, McGraw-Hill Book Co., Inc., New York, 1960.

## LIST OF SYMBOLS

$A_j$	Total area of injection ports at peripheral wall of 2144-port-injection vortex tube, $\text{ft}^2$
$D$	Diameter of vortex tube, ft
$L$	Length of vortex tube, ft
$n_\Gamma$	Exponent in equation $v_\phi \propto r^{(n_\Gamma-1)}$ , where $n_\Gamma = 2 - \text{Re}_{r,p}$
$N_i$	Inner porous tube rotational speed, rpm
$N_o$	Peripheral-wall rotational speed, rpm
$Q_i$	Volumetric flow rate through four slots in nonaxial-flow end wall (see Appendix), $\text{ft}^3/\text{sec}$
$Q_j$	Volumetric flow rate of injection jet which drives vortex, $\text{ft}^3/\text{sec}$
$Q_s$	Volumetric flow rate through one end-wall suction annulus (see Appendix), $\text{ft}^3/\text{sec}$
$Q_t$	Volumetric flow rate through inner porous tube or thru-flow ports, $\text{ft}^3/\text{sec}$
$Q_z$	Volumetric flow rate through axial-flow exhaust annulus, $\text{ft}^3/\text{sec}$
$r$	Local radius from centerline of vortex tube, ft or in.
$r_o$	Outer radius of vortex tube, ft or in.
$\text{Re}_r$	Radial Reynolds number (negative for radial outflow), $Q_t / 2\pi\nu L$ , dimensionless
$\text{Re}_{r,i}$	End-wall injection radial Reynolds number based on injection flow rate through four slots in nonaxial-flow end wall, $Q_i / 2\pi\nu L$ , dimensionless (2144-port-injection vortex tube only; see Appendix)
$\text{Re}_{r,p}$	Local radial Reynolds number in primary-flow region, $(v_r r) / \nu$ , dimensionless
$\text{Re}_{r,s}$	End-wall suction radial Reynolds number based on total suction flow rate through 3/8-in.-wide annulus at $r = 3$ in. in both end walls, $2Q_s / 2\pi\nu L$ , dimensionless (2144-port-injection vortex tube only; see Appendix)

$Re_{t,j}$	Tangential injection Reynolds number based on average injection velocity in 2144-port-injection vortex tube (see Appendix), $V_j r_o / \nu = Q_j r_o / A_j \nu$ , dimensionless
$Re_{t,o}$	Tangential Reynolds number based on peripheral-wall rotational speed, $\pi N_o r_o^2 / 30\nu$ , dimensionless
$Re_{z,w}$	Axial-flow Reynolds number, $Q_z / (7/16)\pi r_o \nu$ , dimensionless
$t$	Time, sec
$V_j$	Average tangential injection velocity in 2144-port-injection vortex tube (see Appendix), $Q_j / A_j$ , ft/sec
$V_r$	Local radial velocity, ft/sec
$V_\phi$	Tangential velocity, ft/sec
$V_{\phi,o}$	Tangential velocity of rotating peripheral wall, $\pi N_o r_o / 30$ , ft/sec
$\bar{V}_{z,w}$	Average axial velocity through annular region having an area equal to 7/16 of tube cross-sectional area, $Q_z / (7/16)\pi r_o^2$
$z$	Distance measured in a direction parallel to the axis of the vortex tube from right end wall or nonaxial-flow end wall, in.
$\epsilon$	Total (laminar plus eddy) viscosity, $ft^2/sec$
$\mu$	Laminar viscosity, $lb\text{-sec}/ft^2$
$\nu$	Kinematic viscosity, $ft^2/sec$
$\rho$	Density of water, $slug/ft^3$
$\phi$	Azimuthal coordinate

## APPENDIX

### RESULTS OF RADIAL-OUTFLOW TESTS IN THE

#### 2144-PORT-INJECTION VORTEX TUBE

Prior to conducting tests in the rotating-peripheral-wall vortex tube, tests were conducted in the 2144-port-injection vortex tube of Ref. 2. The objective of these tests was to determine the influence of increased tangential velocities near the vortex centerline on the turbulence in radial-outflow vortexes. The inner porous tube was rotated at various speeds to vary the tangential velocities in the central region. A brief description of the 2144-port-injection vortex tube is given in the section of this report entitled DESCRIPTION OF EQUIPMENT AND PROCEDURES; a detailed description is given in Ref. 2. Sketches of the fluid injection methods that were used are shown in Fig. 29.

#### Results for Basic Vortex Configuration

Flow visualization tests of the basic vortex configuration with fluid injection through the inner porous tube were performed for  $Re_r = 0, -30$  and  $-60$  with inner porous tube rotational speeds of  $N_i = 0, 400, 800, 1200, 1600,$  and  $2000$  rpm. The results show that rotation of the inner porous tube did not reduce turbulence in the primary-flow region of the vortex. Photographs of typical flow patterns showing the effect of inner porous tube rotation for  $Re_r = -60$  are presented in Fig. 30. The photographs show turbulent flow at all radii for  $N_i = 0, 400, 1200,$  and  $2000$  rpm.

Tangential velocity profiles for the same inner porous tube rotation rates but for  $Re_r = -30$  are shown in Fig. 31. The data show the presence of two regions within the vortex tube with different types of tangential velocity profiles. Tangential velocity profiles of the form  $V_\phi \propto 1/r$  existed at radii from 0.5 in. to approximately 3 in., and tangential velocities of the form  $V_\phi \propto r^{n-1}$ , where  $n > 2$ , existed from a radius of approximately 3 in. to the peripheral wall. Flows having tangential velocity profiles of the latter type have been observed to be turbulent in previous tests (Ref. 2) as well as in the present tests.

Since an increase in the tangential velocities in the central region did not reduce turbulence, it appeared that modification of the tangential velocity profiles near the peripheral wall was also required. To achieve this, an attempt was made to establish a weak radial inflow instead of radial outflow over the region from  $r = 3$  in. to the peripheral wall. The plain end walls used with the rotating inner porous tube assembly were modified to include a 3/8-in.-wide suction annulus at a radius of 3 in. through which a portion of the flow was withdrawn. This

configuration is shown in the lower sketch of Fig. 29a. The flow injected through the inner porous tube (amount given by  $Re_r$ ) and the flow withdrawn through the suction annulus (amount given by  $Re_{r,s}$ ) could be adjusted independently.

Flow visualization tests were conducted for several values of  $Re_r$  from 0 to -100,  $Re_{r,s}$  from 0 to 150, and  $N_i$  from 0 to 1200 rpm. Depending on the combination of these parameters, two different types of flow patterns were observed. One type was turbulent at all radii; the patterns were similar to those shown in Fig. 30. The other consisted of two or more well-defined axial vortex rolls (referred to here as "multiple vortexes"). These multiple vortexes (see Fig. 32) extended the complete length of the vortex tube; their centers were at a radius of approximately 3 in. The multiple vortexes had rotation in the same sense as the mean flow (counterclockwise in Fig. 32). Typical multiple-vortex flow patterns for flow conditions with and without inner porous tube rotation, and the corresponding tangential velocities profiles, are shown in Figs. 32 and 33, respectively. Note in Fig. 33 that the tangential velocities in the radial region between 3 in. and the peripheral wall are much larger than the tangential velocities in the same region shown in Fig. 31.

Combinations of  $Re_r$  and  $Re_{r,s}$  that produce multiple-vortex flow patterns for  $N_i = 0$  and 800 rpm are shown in Fig. 34. The shaded regions indicate the combinations of  $Re_r$  and  $Re_{r,s}$  for which multiple-vortex flow patterns were observed. For all other combinations, the flow was turbulent. The effect of inner porous tube rotational speed on the number of multiple vortexes produced for a typical case ( $Re_r = -75$  and  $Re_{r,s} = 150$ ) is shown in Fig. 35. The number of multiple vortexes increased with increased inner porous tube rotational speed.

#### Results for Axial-Flow Vortex Configuration

A similar series of flow visualization tests was conducted for the axial-flow vortex configuration with fluid injection through the rotating inner porous tube. Sketches of the fluid injection methods used are shown in Fig. 29b. The flow was extremely turbulent. It was characterized by large eddies similar to those observed for large values of  $Re_{z,w}$  in tests in the rotating-peripheral-wall apparatus (see, for example, Fig. 24b).

A configuration with swirl injection through an end wall was also tested. In this configuration, shown in the lower sketch of Fig. 29b, the inner porous tube was removed and fluid was injected tangentially through four 1-in.-long jet slots at the nonaxial-flow end wall. The slots extended from  $r = 0.75$  in. to  $r = 1.75$  in. Photographs of typical flow patterns are shown in Fig. 36 for values of the end-wall injection radial Reynolds number of  $Re_{r,i} = 0, 25, 50,$  and  $80$ . Injection using this method appeared to have little effect on the flow; the flow remained turbulent.

TABLE I

Summary of Flow Conditions Investigated Using the Rotating-Peripheral-Wall Vortex Test Apparatus in the Basic Vortex Configuration

See Fig. 3a for Sketches of Fluid Injection Methods  
 Fluid Withdrawn Through Peripheral Wall  
 Peripheral Wall: 10-in.-dia Lucite Tube with 16,000 0.062-in.-dia holes  
 Inner Porous Tube: 1-in.-dia Porous Metal Tube

CONFIGURATION	RADIAL REYNOLDS NUMBER Re <sub>r</sub>	TANGENTIAL REYNOLDS NUMBER Re <sub>t,o</sub>	PERIPHERAL WALL SPEED N <sub>o</sub> , RPM	FLOW PATTERNS*	
				CENTRAL REGION r= 0 to about 2.5 in.	OUTER REGION r=2.5 to 5.0 in.
No inner porous tube, fluid injection through thru-flow ports, each flow condition tested with both stationary and rotating end walls	0	120,000	73	SEW-T, REW-T	SEW-T, REW-T
	↓	240,000	144	↓	↓
	-30	120,000	73	↓	↓
	↓	240,000	144	↓	↓
	-75	120,000	73	↓	↓
	↓	240,000	144	↓	↓
	↓	330,000	200	↓	↓
	↓	410,000	250	↓	↓
Fluid injection through stationary inner porous tube; each flow condition tested with both stationary and rotating end walls	0	120,000	73	SEW-L, REW-L	SEW-L, REW-L
	↓	240,000	144	↓	↓
	-23	67,000	40	↓	SEW-T, REW-L
	↓	100,800	61	↓	↓
	↓	120,000	73	↓	↓
	↓	144,000	87	↓	↓
	↓	168,000	101	↓	↓
	↓	198,000	120	↓	↓
	↓	240,000	144	↓	↓
	↓	276,000	169	↓	↓
	↓	300,000	183	↓	↓
	↓	324,000	197	SEW-L, REW-O SEW-L, REW-T SEW-L, REW-L	SEW-T, REW-O SEW-T, REW-T SEW-T, REW-L
	-30	67,000	40	↓	↓
	↓	100,800	61	↓	↓
	↓	120,000	73	↓	↓
	↓	144,000	87	↓	↓
	↓	168,000	101	↓	↓
	↓	198,000	120	↓	↓
	↓	240,000	144	↓	↓
	↓	276,000	169	↓	↓
	↓	300,000	183	SEW-L, REW-O SEW-L, REW-T SEW-L, REW-PO	SEW-T, REW-O SEW-T, REW-T SEW-T, REW-PO
	-37.5	67,000	40	↓	↓
	↓	100,800	61	↓	↓
	↓	120,000	73	↓	↓
	↓	144,000	87	↓	↓
	↓	168,000	101	↓	↓
	↓	198,000	120	↓	↓
	↓	240,000	144	↓	↓
	↓	276,000	169	SEW-L, REW-O SEW-L, REW-T SEW-L, REW-PT	SEW-T, REW-O SEW-T, REW-T SEW-T, REW-PT
	-45	67,000	40	↓	↓
	↓	100,800	61	↓	↓
	↓	120,000	73	↓	↓
	↓	144,000	87	↓	↓
	↓	168,000	101	↓	↓
	↓	198,000	120	↓	↓
	↓	240,000	144	↓	↓
	↓	276,000	169	↓	↓
	↓	312,000	190	SEW-L, REW-O SEW-L, REW-T SEW-L, REW-PT	SEW-T, REW-O SEW-T, REW-T SEW-T, REW-PT
	-55	67,000	40	↓	↓
	↓	100,800	61	SEW-L, REW-PT	SEW-T, REW-PT
	↓	120,000	73	↓	↓
	↓	144,000	87	↓	↓
	↓	168,000	101	↓	↓
	↓	198,000	120	↓	↓
	↓	240,000	144	SEW-L, REW-T SEW-L, REW-PT	SEW-T, REW-T SEW-T, REW-PT
-75	67,000	40	↓	↓	
↓	100,800	61	↓	↓	
↓	120,000	73	↓	↓	
↓	144,000	87	↓	↓	
↓	160,000	97	SEW-L, REW-T SEW-L, REW-PT	SEW-T, REW-T SEW-T, REW-PT	
-105	67,000	40	↓	↓	
↓	104,000	63	↓	↓	
↓	120,000	73	↓	↓	
↓	133,000	81	SEW-L, REW-T	SEW-T, REW-T	

\*For stationary end walls (SEW) or rotating end walls (REW):  
 L = Laminar  
 O = Oscillating between laminar and turbulent  
 PO = Partly oscillating between laminar and turbulent  
 PT = Partly turbulent  
 T = Turbulent

Continued

TABLE I (Concluded)

CONFIGURATION	RADIAL REYNOLDS NUMBER $Re_r$	TANGENTIAL REYNOLDS NUMBER $Re_{t,o}$	PERIPHERAL WALL SPEED $N_o$ , RPM	INNER TUBE SPEED $N_i$ , RPM	$N_o/N_i$	END WALL CONFIGURATION	FLOW PATTERNS
Fluid injection through rotating inner porous tube; end wall configuration denoted by (SEW) stationary end walls or (REW) rotating end walls	0	120,000	73	73	1.00	SEW & REW	All flow patterns turbulent in both central and outer regions
	-45	120,000	73	73	1.00	SEW & REW	
		120,000	73	260	0.281	SEW & REW	
		240,000	144	35	4.114	SEW	
		240,000	144	73	1.973	SEW	
		240,000	144	400	0.360	SEW	
		240,000	144	600	0.240	SEW & REW	
		327,000	195	195	1.00	SEW	
		327,000	195	600	0.325	SEW & REW	
		327,000	195	740	0.264	SEW	
		327,000	195	469	0.416	REW	
	-75	120,000	73	73	1.00	REW	
		240,000	144	144	1.00	REW	
		240,000	144	400	0.360	REW	
		240,000	144	520	0.277	REW	
		240,000	144	650	0.222	REW	
		324,000	197	620	0.318	REW	
		384,000	234	620	0.377	REW	

TABLE II

Summary of Flow Conditions Investigated Using the Rotating-Peripheral-Wall Vortex Test Apparatus in the Axial-Flow Vortex Configuration

See Fig. 3b for Sketches of Fluid Injection Methods  
 Fluid Withdrawn Through 3/4-In.-Wide Annulus Near Outer Edge of Axial-Flow End Wall  
 All Flow Conditions Tested with both Stationary and Rotating End Walls  
 Peripheral Wall: 10-in.-dia Lucite Tube with 16,000 0.062-in.-dia holes  
 Inner Porous Tube: 1-in.-dia Porous Metal Tube

CONFIGURATION	AXIAL-FLOW REYNOLDS NUMBER $Re_{z,w}$	TANGENTIAL REYNOLDS NUMBER $Re_r$	RADIAL REYNOLDS NUMBER $Re_{t,o}$	$v_{z,w} / v_{\phi,o}$	PERIPHERAL WALL SPEED $N_o$ , RPM	INNER TUBE SPEED $N_i$ , RPM	FLOW PATTERNS* CENTRAL REGION $r = 0$ to about 2.5 in.	OUTER REGION $r = 2.5$ to 5.0 in.		
Fluid injection through inner porous tube only	880	67,000	-30	0.0131	40	0	O	T		
	↓	120,000	↓	0.0073	73	0	L	↓		
		198,000		0.0044	120	0	L			
		240,000		0.0037	144	0	L			
		288,000		0.0030	175	0	L			
	1,310	67,000	-45	0.0196	40	0	O	L		
	↓	120,000	↓	0.0109	73	0	L	↓		
		198,000		0.0066	120	0	L			
		240,000		0.0054	144	0	L			
		288,000		0.0045	175	0	L			
	↓	120,000	↓	0.0109	73	500	T	↓		
		240,000		0.0054	144	600	T			
		327,000		0.0040	195	600	T			
		67,000		-75	0.0328	40	0		O	
	↓	120,000	↓	0.0183	73	0	O	↓		
		198,000		0.0111	120	0	L			
		240,000		0.0092	144	0	L			
		288,000		0.0076	175	0	L			
	3,180	67,000	-115	0.0475	40	0	T	L		
	↓	120,000	↓	0.0265	73	0	T	↓		
		198,000		0.0161	120	0	T			
		288,000		0.0110	175	0	T			
		67,000		-150	0.0634	40	0		T	
	↓	198,000	↓	0.0215	120	0	T	↓		
327,000		0.0130		195	600	T				
880		67,000		0	0.0131	40	0		O	T
↓		120,000		↓	0.0073	73	0		L	↓
	198,000	0.0044	120		0	L				
	240,000	0.0037	144		0	L				
	288,000	0.0030	175		0	L				
1,310	67,000	0	0.0196	40	0	O	L			
↓	120,000	↓	0.0109	73	0	L	↓			
	198,000		0.0066	120	0	L				
	240,000		0.0054	144	0	L				
	288,000		0.0045	175	0	L				
↓	120,000	↓	0.0421	40	0	T	↓			
	198,000		0.0235	73	0	T				
	288,000		0.0142	120	0	T				
	67,000		0.0098	175	0	T				
5,650	67,000	0	0.0843	40	0	T	L			
↓	120,000	↓	0.0471	73	0	T	↓			
	198,000		0.0285	120	0	T				
	288,000		0.0196	175	0	T				
	67,000		0.209	40	0	T				
↓	188,000	↓	0.0745	112	0	T	↓			
	188,000		0.0745	112	600	T				
	188,000		0.313	40	0	T				
	67,000		0.175	73	0	T				
14,000	148,000	0	0.142	90	0	T	L			
↓	198,000	↓	0.106	120	0	T	↓			
	240,000		0.0875	144	0	T				
	288,000		0.0729	175	0	T				
	329,000		0.0638	200	0	T				
↓	120,000	↓	0.175	73	800	T	↓			
	120,000		0.175	73	600	T				

\* For both stationary and rotating end walls:  
 L = Laminar  
 O = Oscillating between laminar and turbulent  
 T = Turbulent

Continued

TABLE II (Concluded)

CONFIGURATION	AXIAL-FLOW REYNOLDS NUMBER $Re_{z,w}$	TANGENTIAL REYNOLDS NUMBER $Re_r$	RADIAL REYNOLDS NUMBER $Re_{t,o}$	$V_{z,w}/V_{\phi,o}$	PERIPHERAL WALL SPEED $N_o$ , RPM	INNER TUBE SPEED $N_i$ , RPM	FLOW PATTERNS*	
							CENTRAL REGION $r = 0$ to about 2.5 in.	OUTER REGION $r = 2.5$ to 5.0 in.
Fluid injection through peripheral wall and inner porous tube	1,760	67,000	-30	0.0263	40	0	0	T
		120,000		0.0147	73	0	0	
		198,000		0.0089	120	0	L	
		288,000		0.0061	175	0	L	
	2,620	120,000	-45	0.0218	73	0	T	
		240,000		0.0109	144	0	L	
	2,790	67,000	-30	0.0416	40	0	T	
		120,000		0.0232	73	0		
		148,000		0.0188	90	0		
		197,000		0.0142	120	0		
		240,000		0.0116	144	0		
		288,000		0.0097	175	0		
		329,000		0.0085	200	0		
		394,000		0.0071	240	0		
	3,530	67,000	-60	0.0527	40	0		
		120,000		0.0294	73	0		
		198,000		0.0178	120	0		
		288,000		0.0122	175	0		
	4,750	67,000	-30	0.0709	40	0		
		120,000		0.0396	73	0		
		148,000		0.0321	90	0		
		198,000		0.0240	120	0		
		240,000		0.0198	144	0		
		288,000		0.0165	175	0		
		329,000		0.0144	200	0		
		394,000		0.0120	240	0		
	9,680	67,000		0.144	40	0		
		120,000		0.0807	73	0		
		148,000		0.0654	90	0		
		198,000		0.0489	120	0		
		240,000		0.0403	144	0		
		288,000		0.0336	175	0		
		329,000		0.0294	200	0		
		394,000		0.0240	240	0		
	14,000	67,000	-45	0.209	40	0		
		94,000		0.149	56	0		
		188,000		0.0745	112	0		
		281,000		0.0498	168	0		
	21,000	67,000		0.313	40	0		
		120,000		0.175	73	0		
	148,000		0.142	90	0			
	198,000		0.106	120	0			
	240,000		0.0875	144	0			
	288,000		0.0729	175	0			
	329,000		0.0638	200	0			
	394,000		0.0533	240	0			
	67,000	-75	0.313	40	0			
	120,000		0.175	73	0			
	148,000		0.142	90	0			
	198,000		0.106	120	0			
	240,000		0.0875	144	0			
	288,000		0.0729	175	0			
	329,000		0.0638	200	0			
No inner porous tube; fluid injection through peripheral wall and fluid withdrawal through thru-flow ports at centers of end walls (not shown in Fig. 3b)	16,600	67,000	+75	0.248	40	0	L	T
		83,000	+75	0.200	50	0	L	
		67,000	+90	0.248	40	0	L	

\* For both stationary and rotating end walls:  
 L = Laminar  
 0 = Oscillating between laminar and turbulent  
 T = Turbulent

# ROTATING - PERIPHERAL - WALL WATER - VORTEX TEST APPARATUS

INNER POROUS TUBE NOT INSTALLED

INNER - POROUS - TUBE DRIVE  
END - WALL DRIVE SPOOL  
PERIPHERAL - WALL DRIVE  
PERIPHERAL WALL (DIA = 10 IN.)  
PLENUM (DIA = 14 IN.)

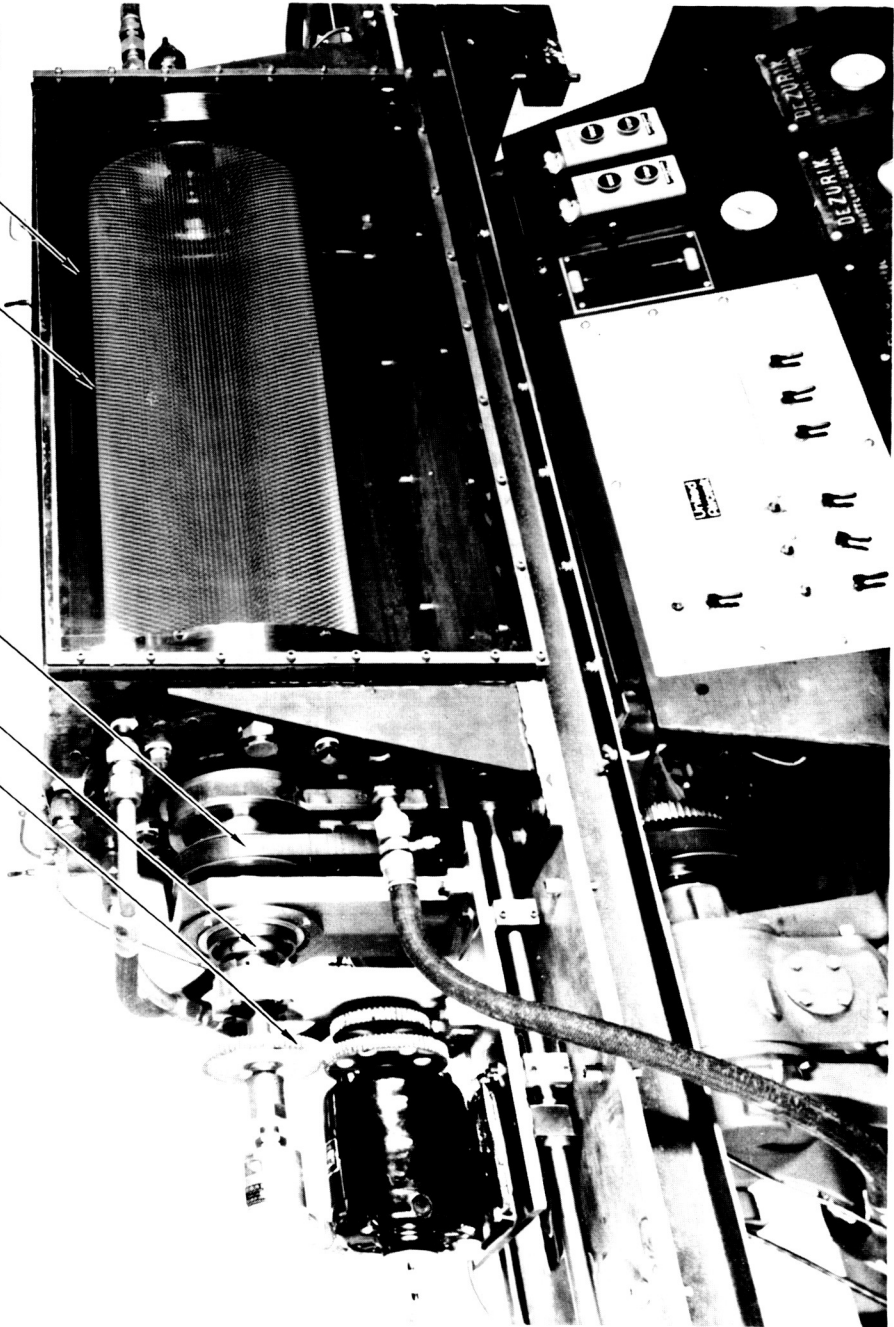
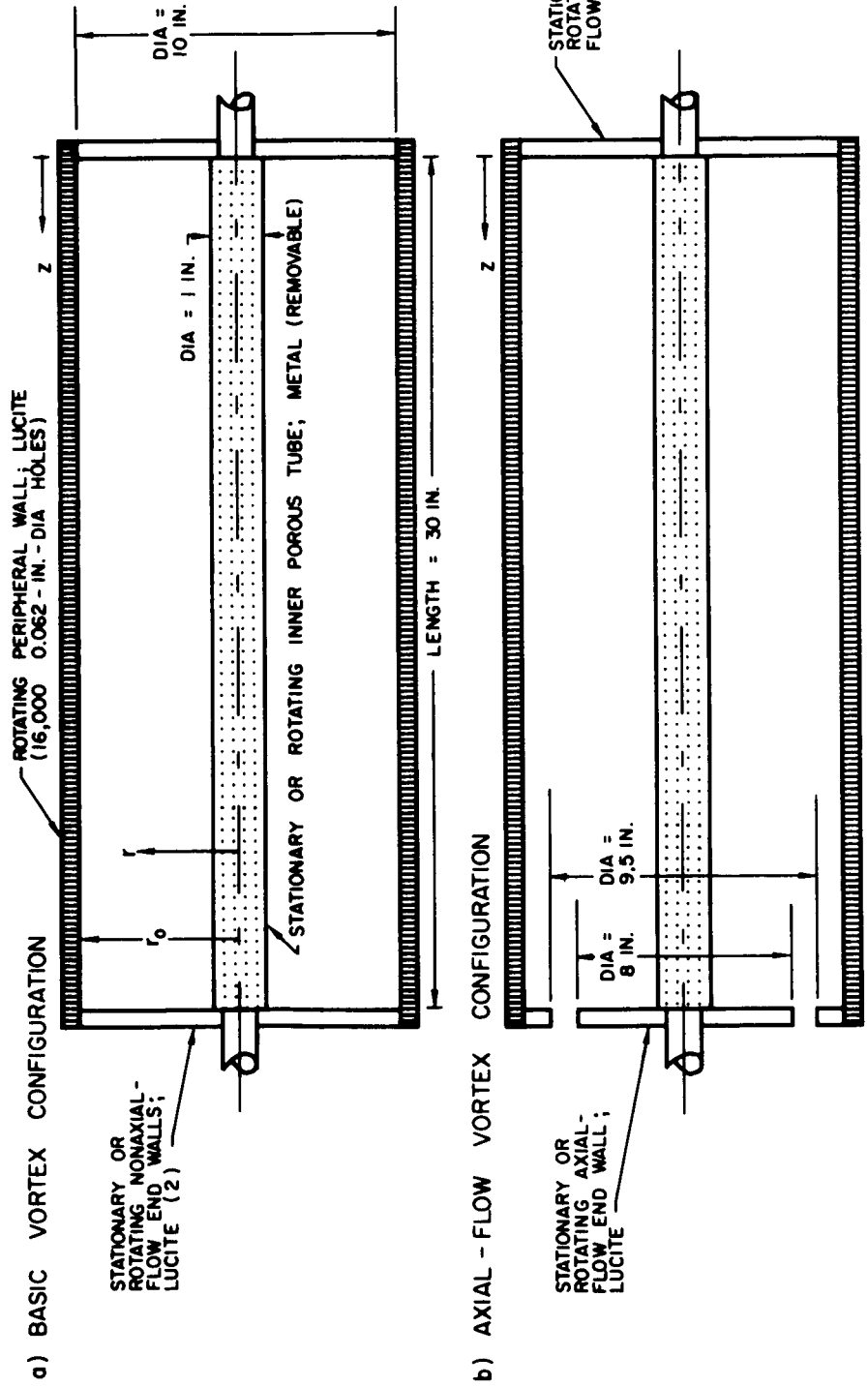


FIG. 1

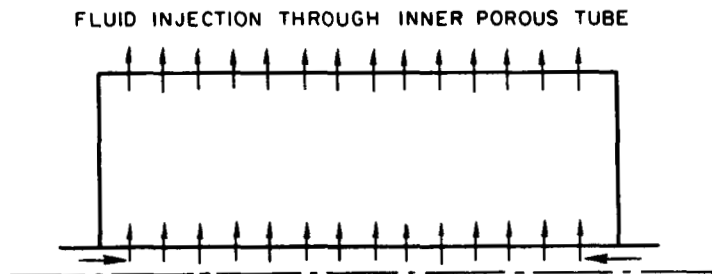
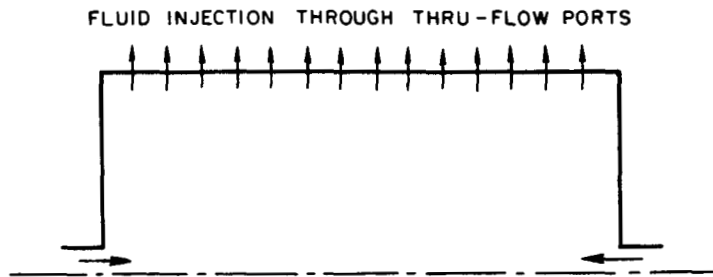
DETAILS OF VORTEX TUBE CONFIGURATIONS USED IN TESTS

SKETCHES CORRESPOND TO FRONT-VIEW PHOTOGRAPH IN FIG. 1

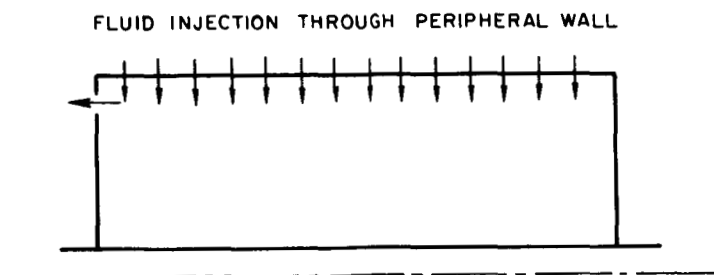
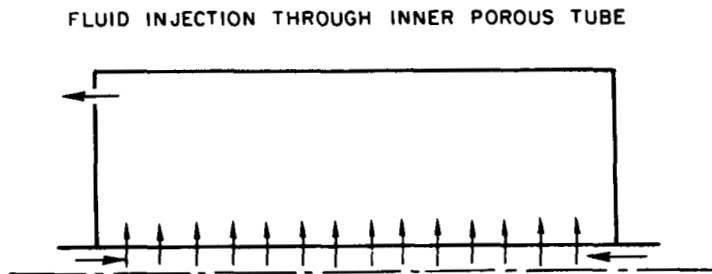


SKETCHES OF FLUID INJECTION METHODS USED  
IN ROTATING-PERIPHERAL-WALL VORTEX TEST APPARATUS

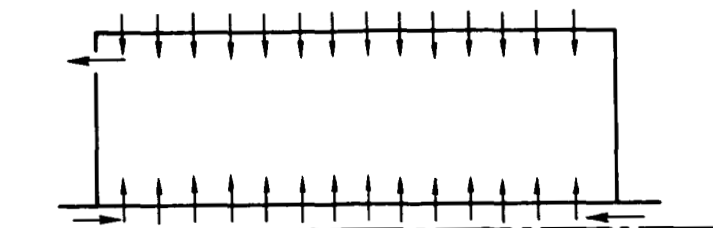
a) BASIC VORTEX CONFIGURATION



b) AXIAL-FLOW VORTEX CONFIGURATION



FLUID INJECTION THROUGH PERIPHERAL WALL AND INNER POROUS TUBE



# OPTICAL SYSTEM USED TO OBTAIN DYE AND PARTICLE - TRACE PHOTOGRAPHS

NOTE: (1) FOR PHOTOGRAPHS TAKEN THROUGH END WALL, (SEE SKETCH) ILLUMINATION OF DYE AND NEUTRALLY BUOYANT PARTICLES WAS BY LIGHT PASSING THROUGH AXIAL MID-PLANE

(2) FOR DYE PHOTOGRAPHS THROUGH SIDE OF VORTEX TUBE, LOCATIONS OF CAMERA AND LIGHT SOURCE WERE INTERCHANGED

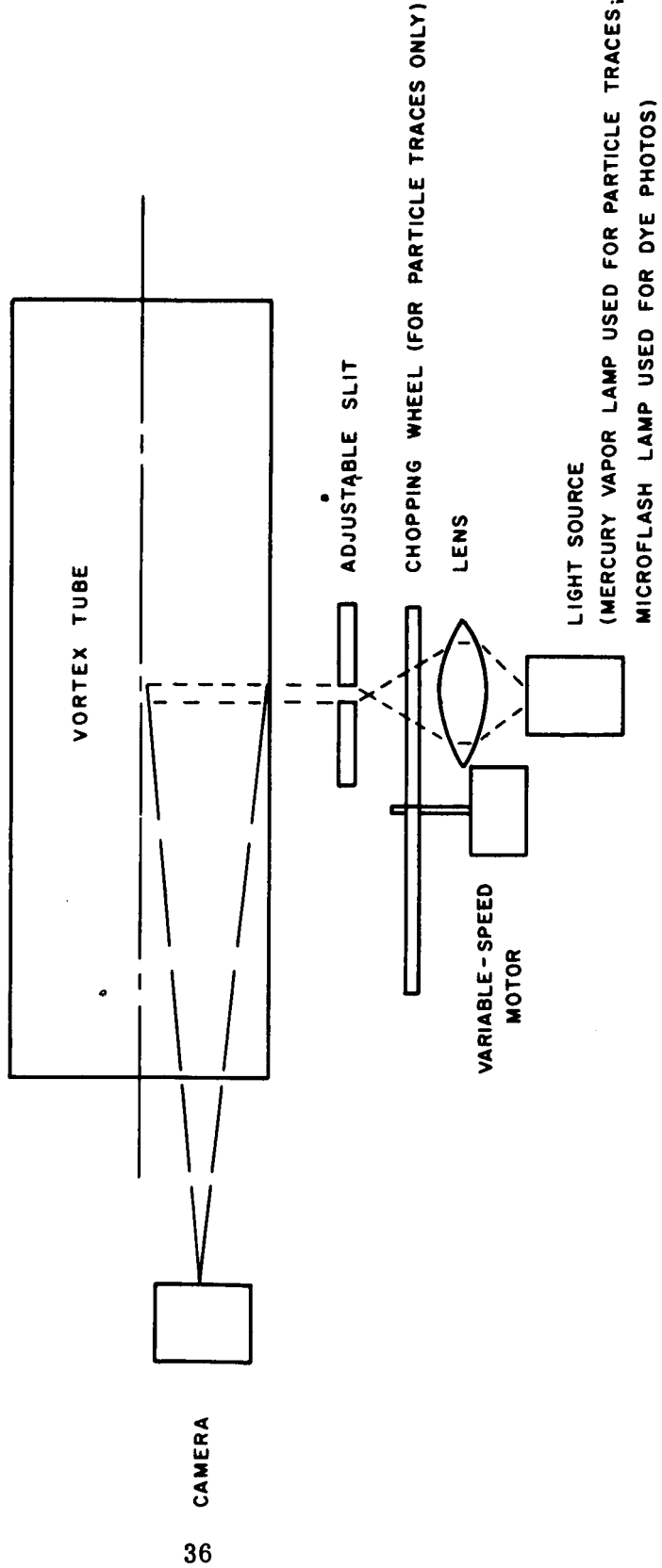
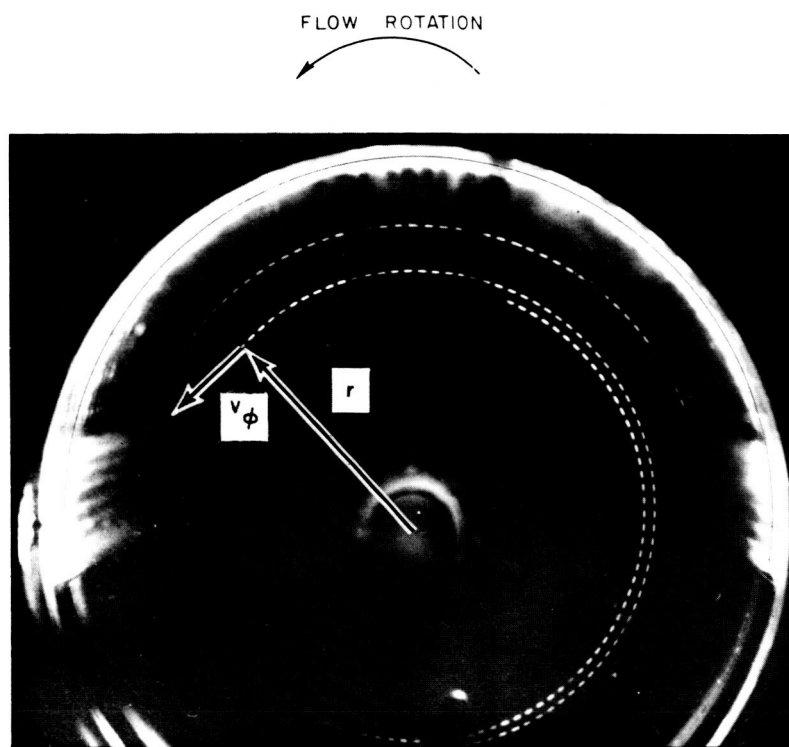


FIG. 4

TYPICAL PARTICLE-TRACE PHOTOGRAPH

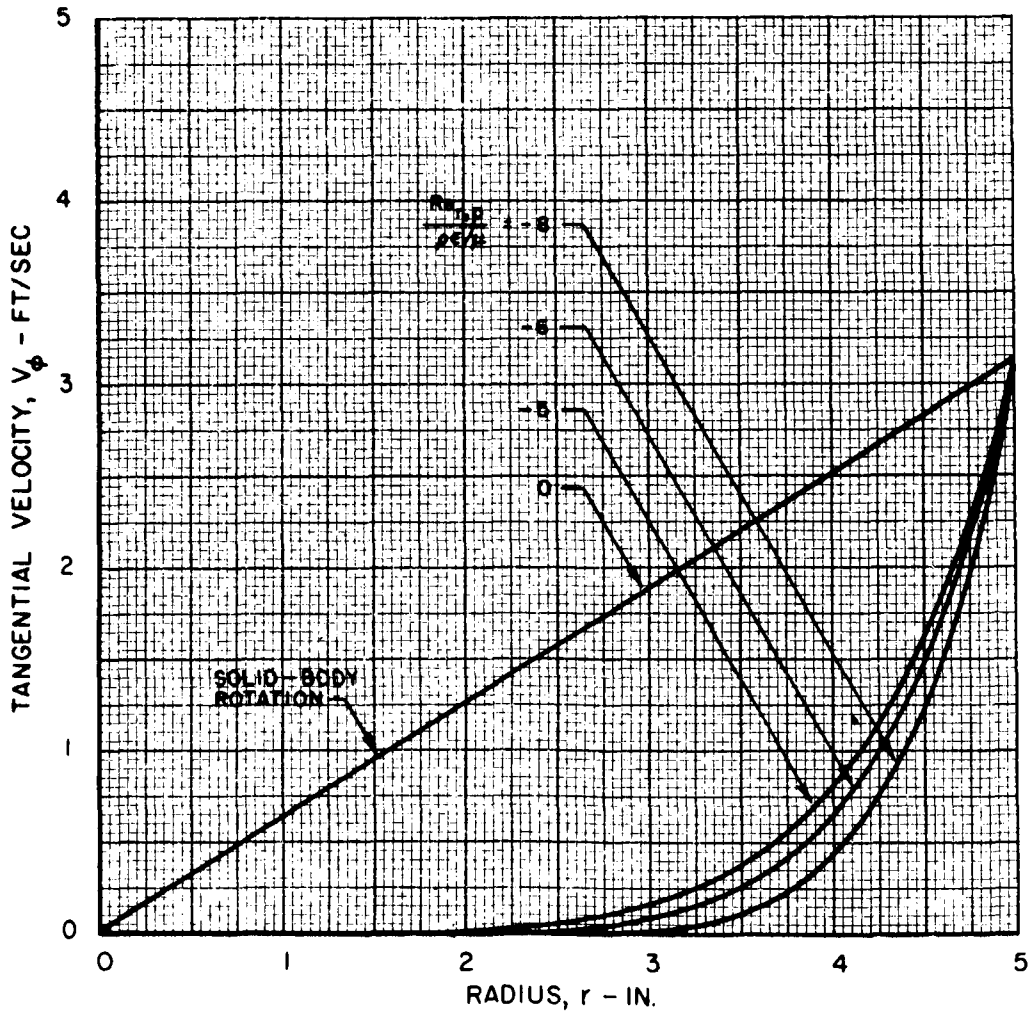


THEORETICAL RADIAL-OUTFLOW TANGENTIAL VELOCITY PROFILES FOR ROTATING FLOWS WITHOUT SUPERIMPOSED AXIAL FLOW

$$v_{\phi} \propto r^{(n_{\Gamma}-1)}$$

IF  $Re_{r,p}$  AND  $\rho\epsilon/\mu$  ARE INDEPENDENT OF RADIUS,  $n_{\Gamma} = 2 - Re_{r,p} / \frac{\rho\epsilon}{\mu}$

FOR LAMINAR FLOW,  $\rho\epsilon/\mu = 1.0$



COMPARISON OF TYPICAL FLOW PATTERNS IN ROTATING-PERIPHERAL-WALL AND 2144-PORT-INJECTION VORTEX TUBES

BASIC VORTEX CONFIGURATION

STATIONARY END WALLS

SEE FIG. 8 FOR CORRESPONDING TANGENTIAL VELOCITY PROFILES

FLOW ROTATION

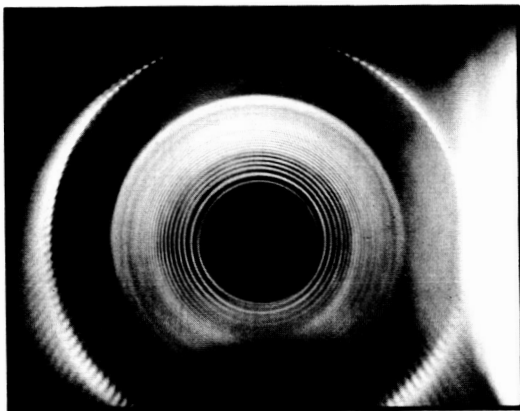


a) ROTATING-PERIPHERAL-WALL VORTEX TUBE,

$N_0 = 73$  RPM

$Re_r = 0$       $Re_{t,o} = 120,000$

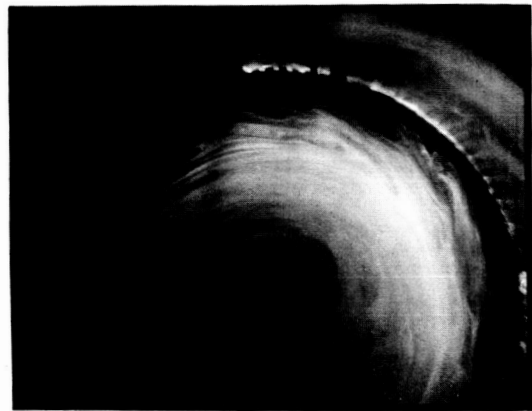
NO INNER POROUS TUBE



b) 2144-PORT-INJECTION VORTEX TUBE

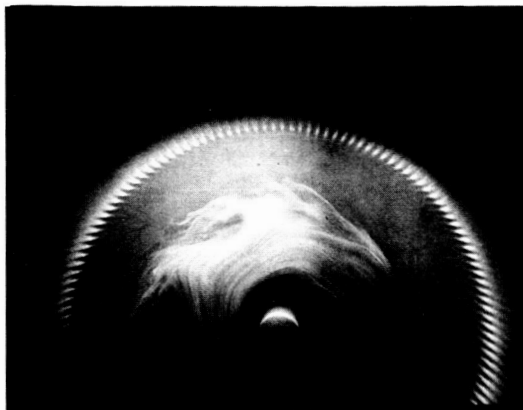
$Re_r = 0$       $Re_{t,j} = 120,000$

NO INNER POROUS TUBE



$Re_r = -20$       $Re_{t,o} = 80,000$

FLUID INJECTION THROUGH STATIONARY  
INNER POROUS TUBE



$Re_r = -20$       $Re_{t,j} = 80,000$

FLUID INJECTION THROUGH STATIONARY  
INNER POROUS TUBE



# COMPARISON OF TYPICAL TANGENTIAL VELOCITY PROFILES IN ROTATING-PERIPHERAL-WALL AND 2144-PORT-INJECTION VORTEX TUBES

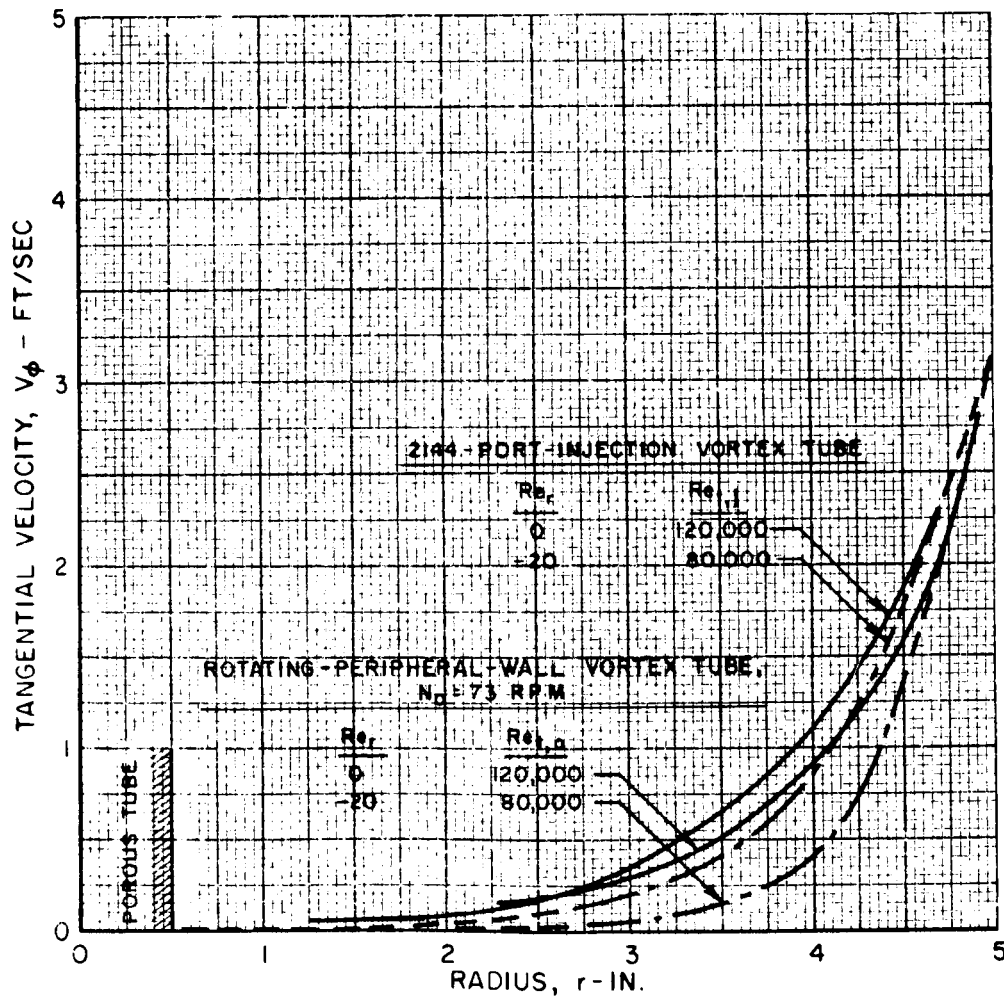
## BASIC VORTEX CONFIGURATION

STATIONARY END WALLS

SEE FIG. 7 FOR CORRESPONDING FLOW PATTERNS

$Re_r = 0$ , NO INNER POROUS TUBE

$Re_r = -20$ , FLUID INJECTION THROUGH STATIONARY INNER POROUS TUBE



COMPARISON OF TYPICAL FLOW PATTERNS FOR FLUID INJECTION THROUGH THRU-FLOW PORTS AND THROUGH STATIONARY INNER POROUS TUBE

BASIC VORTEX CONFIGURATION

RADIAL REYNOLDS NUMBER,  $Re_r = -30$   
 PERIPHERAL-WALL SPEED,  $N_o = 73$  RPM  
 TANGENTIAL REYNOLDS NUMBER,  $Re_{t,o} = 120,000$

FLOW ROTATION



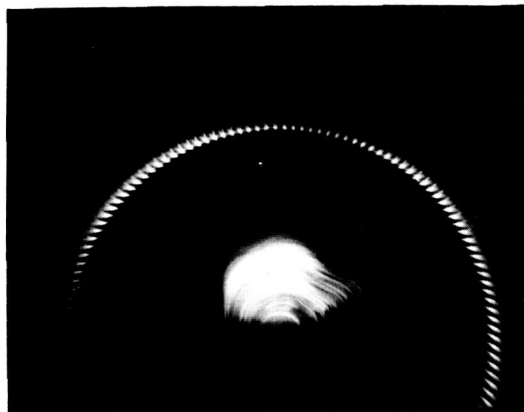
a) FLUID INJECTION THROUGH THRU-FLOW PORTS

STATIONARY END WALLS



b) FLUID INJECTION THROUGH STATIONARY INNER POROUS TUBE

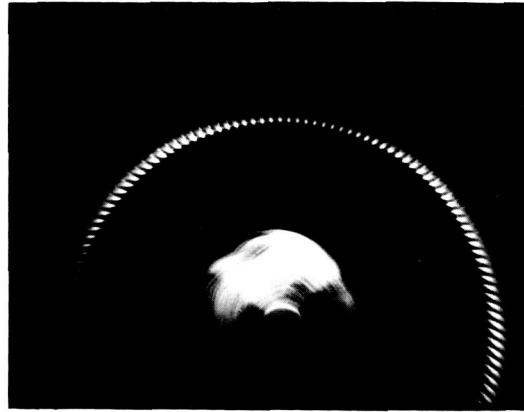
STATIONARY END WALLS



ROTATING END WALLS



ROTATING END WALLS



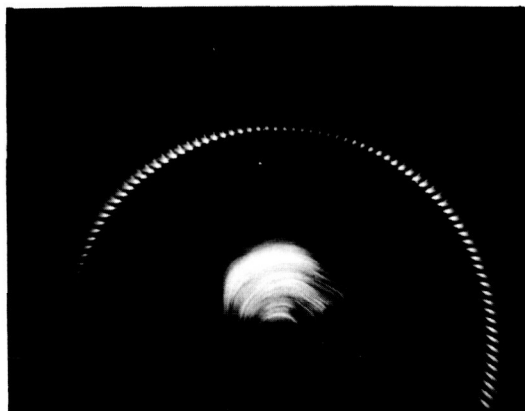
COMPARISON OF TYPICAL FLOW PATTERNS FOR STATIONARY AND ROTATING END WALLS

RADIAL REYNOLDS NUMBER,  $Re_r = -30$   
 FLUID INJECTION THROUGH STATIONARY INNER POROUS TUBE  
 PERIPHERAL-WALL SPEED,  $N_o = 73$  RPM  
 TANGENTIAL REYNOLDS NUMBER,  $Re_{t,o} = 120,000$

FLOW ROTATION



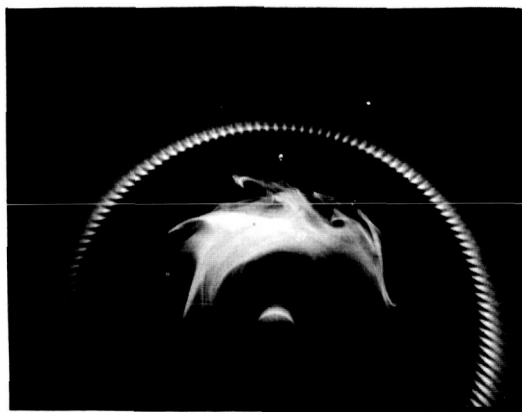
a) STATIONARY END WALLS  
 DYE NEAR CENTER



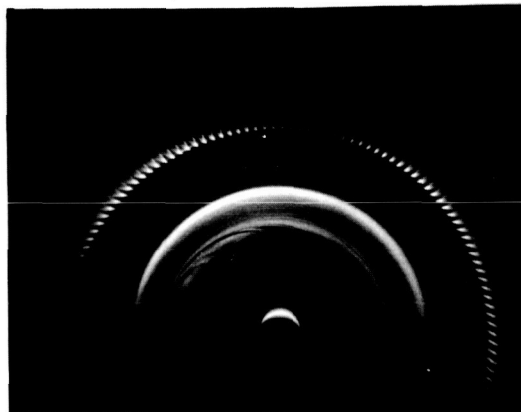
b) ROTATING END WALLS  
 DYE NEAR CENTER



DYE NEAR MID-RADIUS



DYE NEAR MID-RADIUS



# COMPARISON OF TYPICAL TANGENTIAL VELOCITY PROFILES FOR STATIONARY AND ROTATING END WALLS

## BASIC VORTEX CONFIGURATION

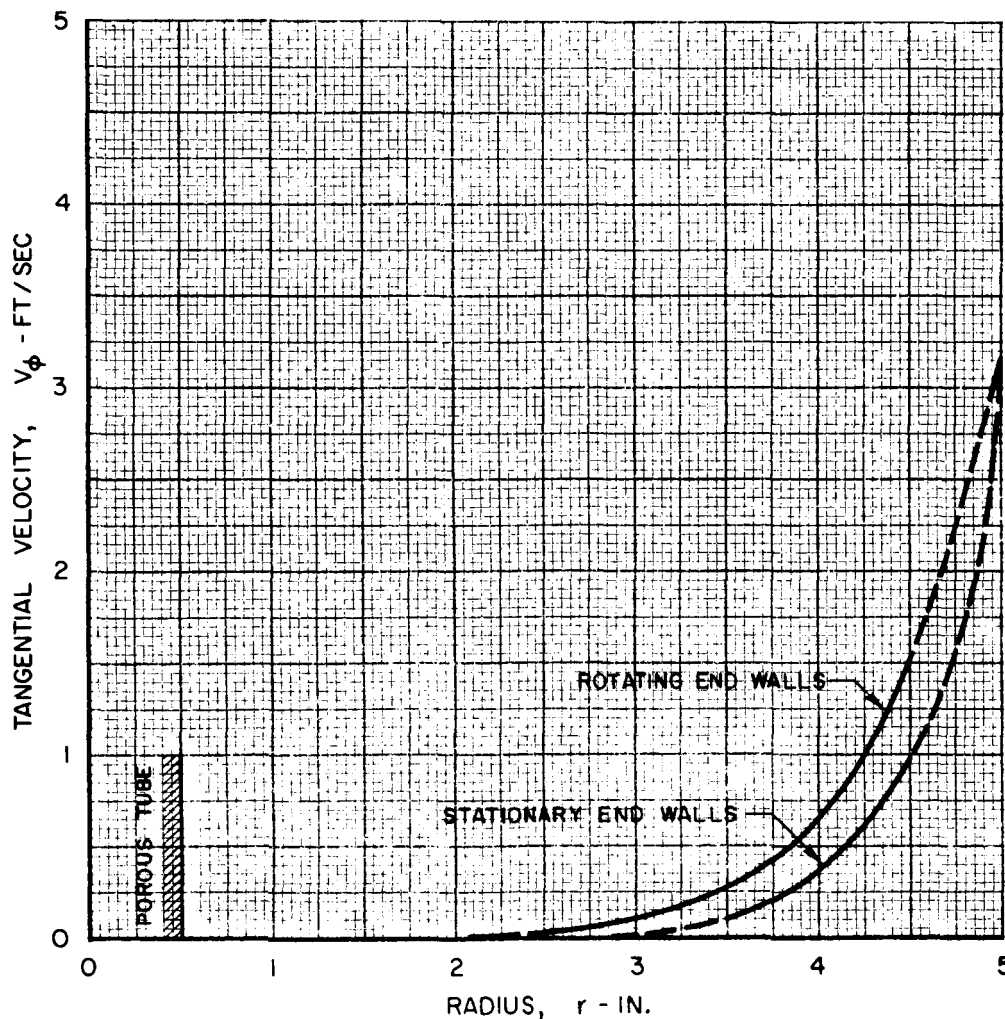
RADIAL REYNOLDS NUMBER,  $Re_r = -30$

FLUID INJECTION THROUGH STATIONARY INNER POROUS TUBE

PERIPHERAL-WALL SPEED,  $N_0 = 73$  RPM

TANGENTIAL REYNOLDS NUMBER,  $Re_{t,0} = 80,000$

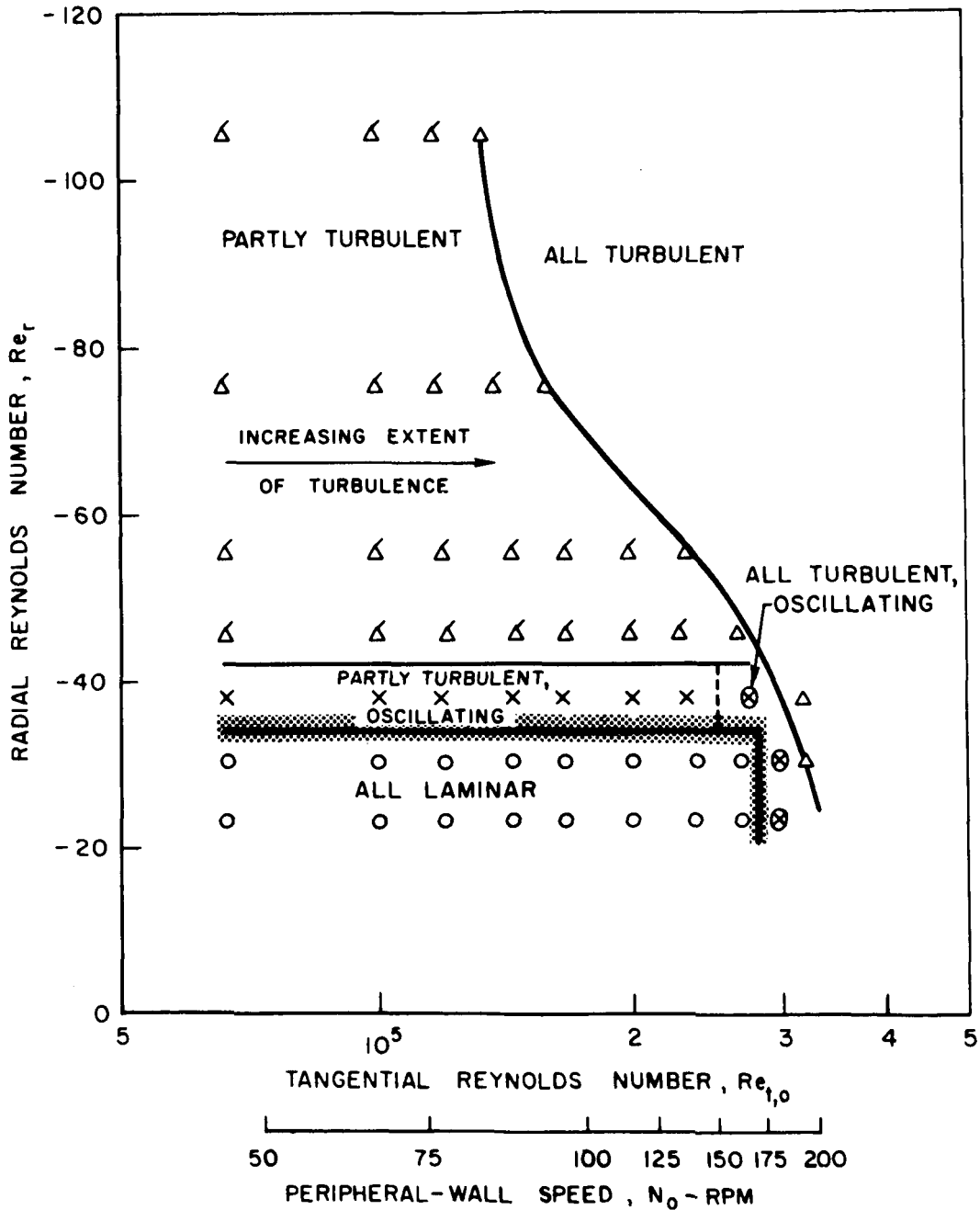
SEE FIG. 10 FOR CORRESPONDING FLOW PATTERNS



SUMMARY OF LAMINAR AND TURBULENT FLOW CONDITIONS  
OBSERVED IN BASIC VORTEX CONFIGURATION

ROTATING-PERIPHERAL-WALL VORTEX TEST APPARATUS

ROTATING END WALLS  
FLUID INJECTION THROUGH STATIONARY INNER POROUS TUBE



# EFFECT OF PERIPHERAL-WALL SPEED ON AXIAL EXTENT OF TURBULENCE

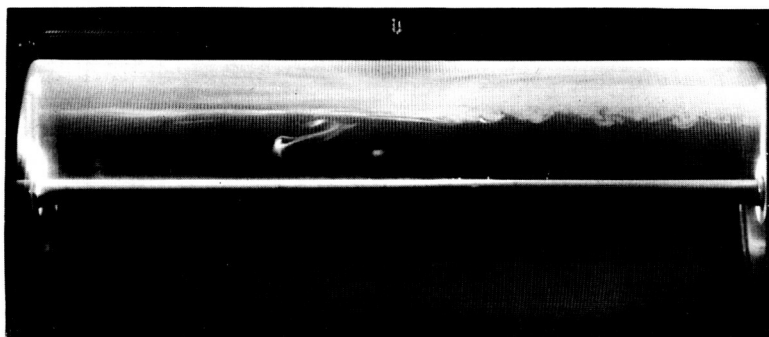
## BASIC VORTEX CONFIGURATION

ROTATING END WALLS

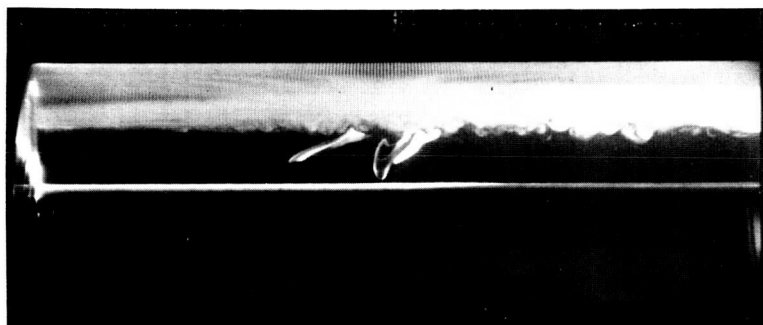
RADIAL REYNOLDS NUMBER,  $Re_r = -45$

FLUID INJECTION THROUGH STATIONARY INNER POROUS TUBE

a) PERIPHERAL-WALL SPEED,  $N_o = 73$  RPM; TANGENTIAL REYNOLDS NUMBER,  $Re_{t,o} = 120,000$



b) PERIPHERAL-WALL SPEED,  $N_o = 156$  RPM; TANGENTIAL REYNOLDS NUMBER,  $Re_{t,o} = 256,000$



# COMPARISON OF TANGENTIAL VELOCITY PROFILES FOR TWO DIFFERENT RADIAL REYNOLDS NUMBERS LEADING TO PARTLY TURBULENT AND COMPLETELY LAMINAR FLOW PATTERNS

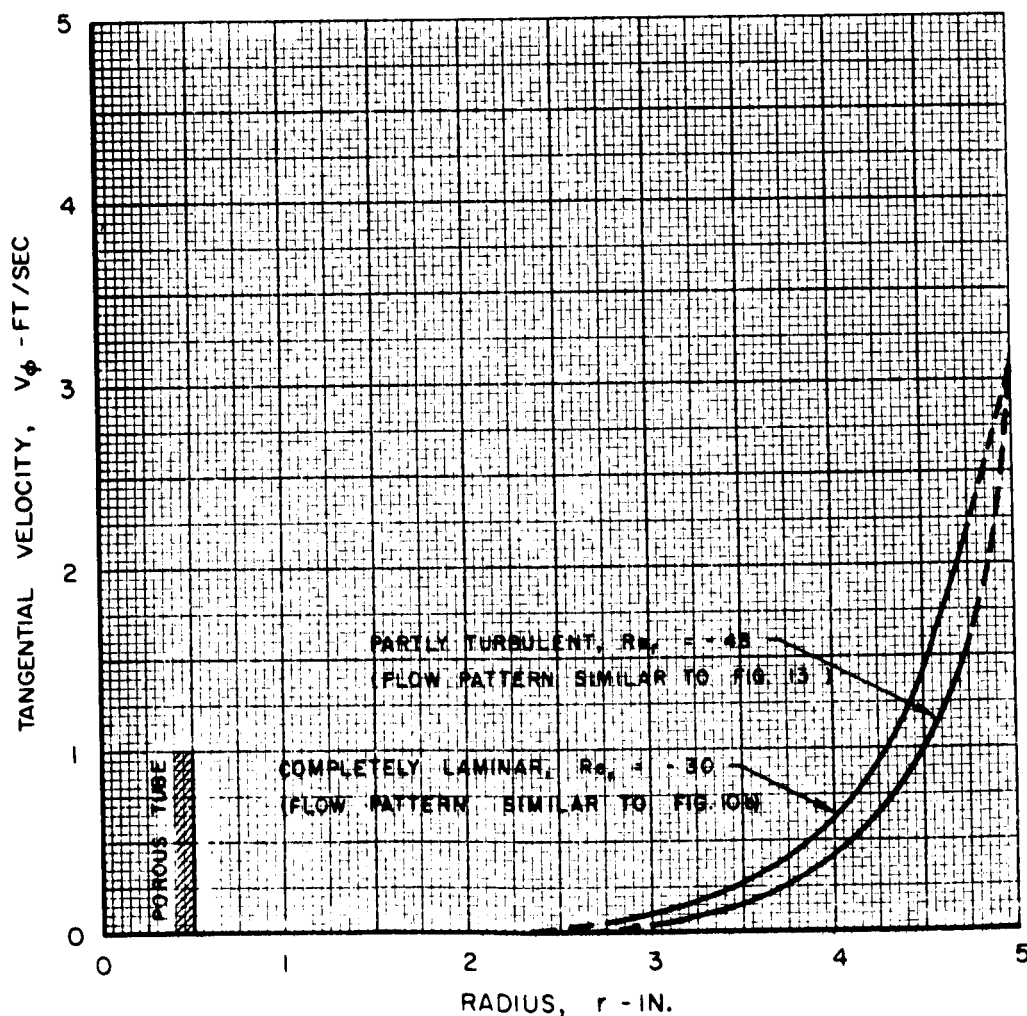
## BASIC VORTEX CONFIGURATION

ROTATING END WALLS

FLUID INJECTION THROUGH STATIONARY INNER POROUS TUBE

PERIPHERAL-WALL SPEED,  $N_0 = 73$  RPM

TANGENTIAL REYNOLDS NUMBER,  $Re_{t,0} = 80,000$

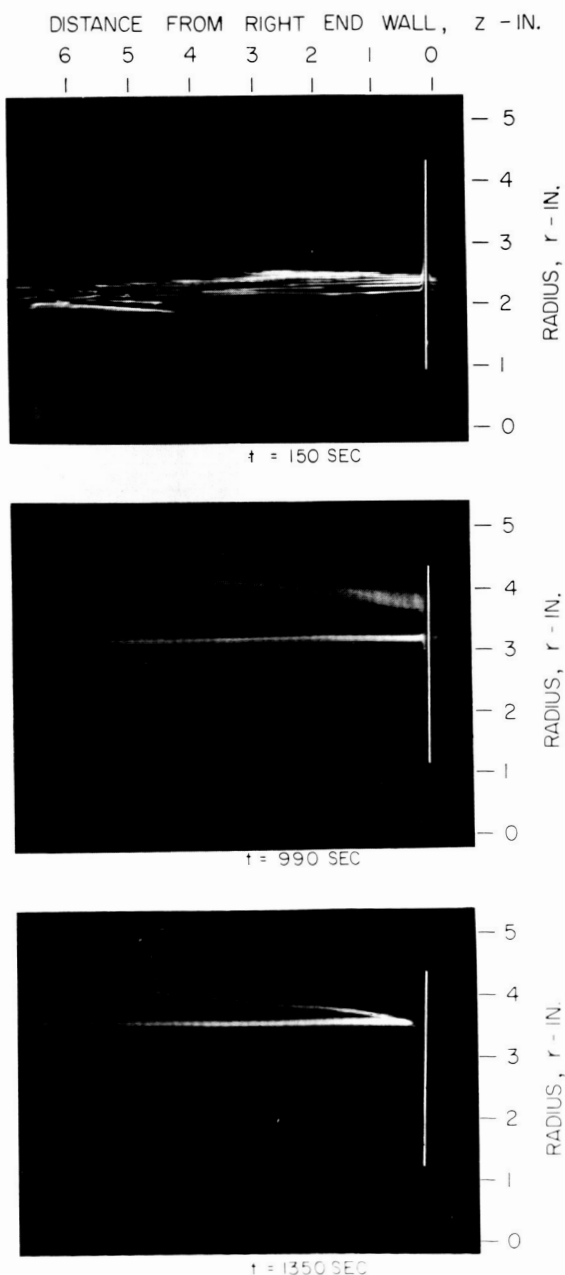


FLOW PATTERNS NEAR RIGHT END WALL SHOWING FLOW INTO AND  
OUT OF END-WALL BOUNDARY LAYER

BASIC VORTEX CONFIGURATION

ROTATING END WALLS  
 RADIAL REYNOLDS NUMBER,  $Re_r = -15$   
 FLUID INJECTION THROUGH STATIONARY INNER POROUS TUBE  
 PERIPHERAL-WALL SPEED,  $N_0 = 110$  RPM  
 TANGENTIAL REYNOLDS NUMBER,  $Re_{t,0} = 117,000$

PHOTOGRAPHS TAKEN AT INDICATED TIMES AFTER CESSATION OF DYE INJECTION THROUGH INNER POROUS TUBE



# VARIATION OF LOCAL RADIAL REYNOLDS NUMBER WITH RADIUS AT AXIAL MID-PLANE FOR FLOW PATTERNS SHOWN IN FIG. 15

## BASIC VORTEX CONFIGURATION

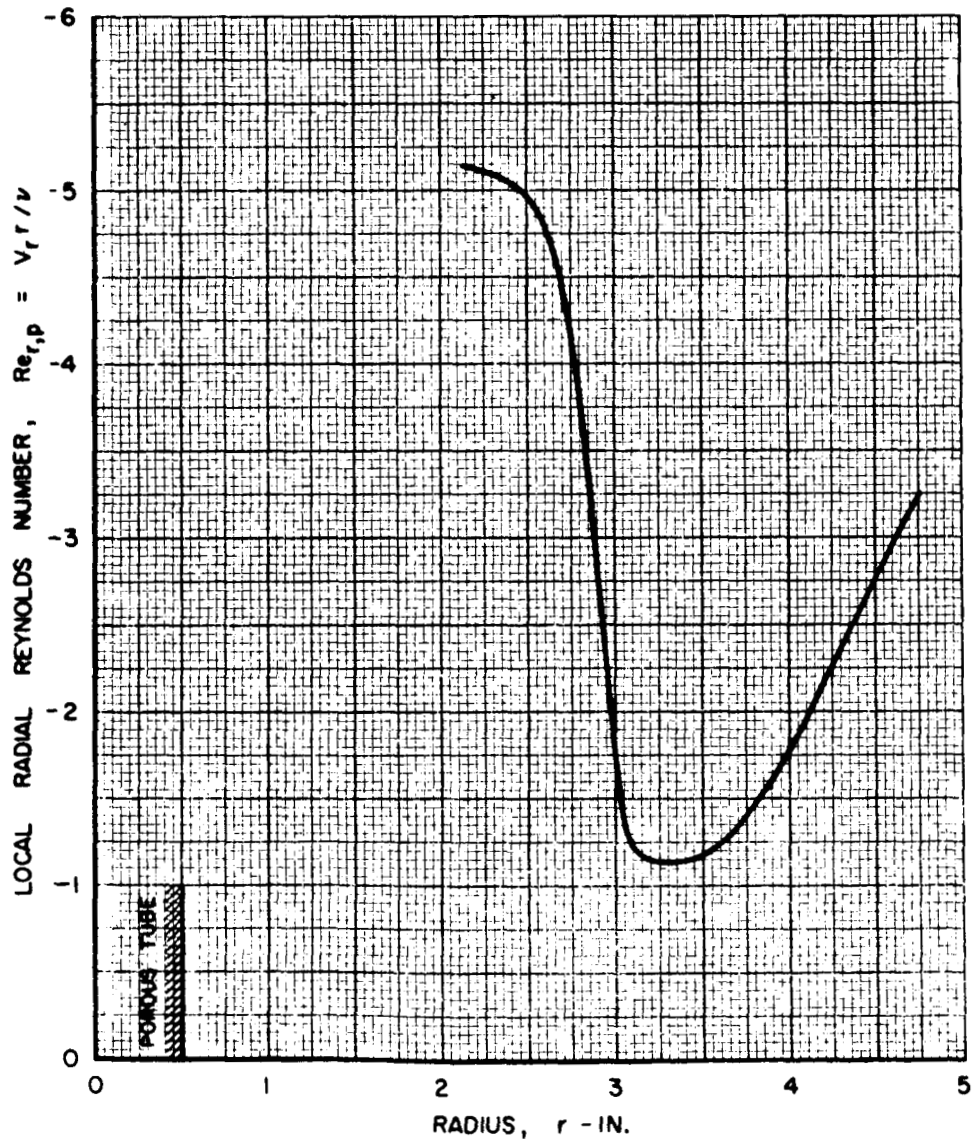
ROTATING END WALLS

RADIAL REYNOLDS NUMBER,  $Re_r = -15$

FLUID INJECTION THROUGH STATIONARY INNER POROUS TUBE

PERIPHERAL-WALL SPEED,  $N_0 = 110$  RPM

TANGENTIAL REYNOLDS NUMBER,  $Re_{t,0} = 117,000$



# SKETCH OF TYPICAL LAMINAR STREAMLINE PATTERN

## BASIC VORTEX CONFIGURATION

ROTATING END WALLS

FLUID INJECTION THROUGH STATIONARY INNER POROUS TUBE

SKETCH BASED ON ANALYSIS OF FLOW PATTERNS SIMILAR TO THOSE OF FIG. 15

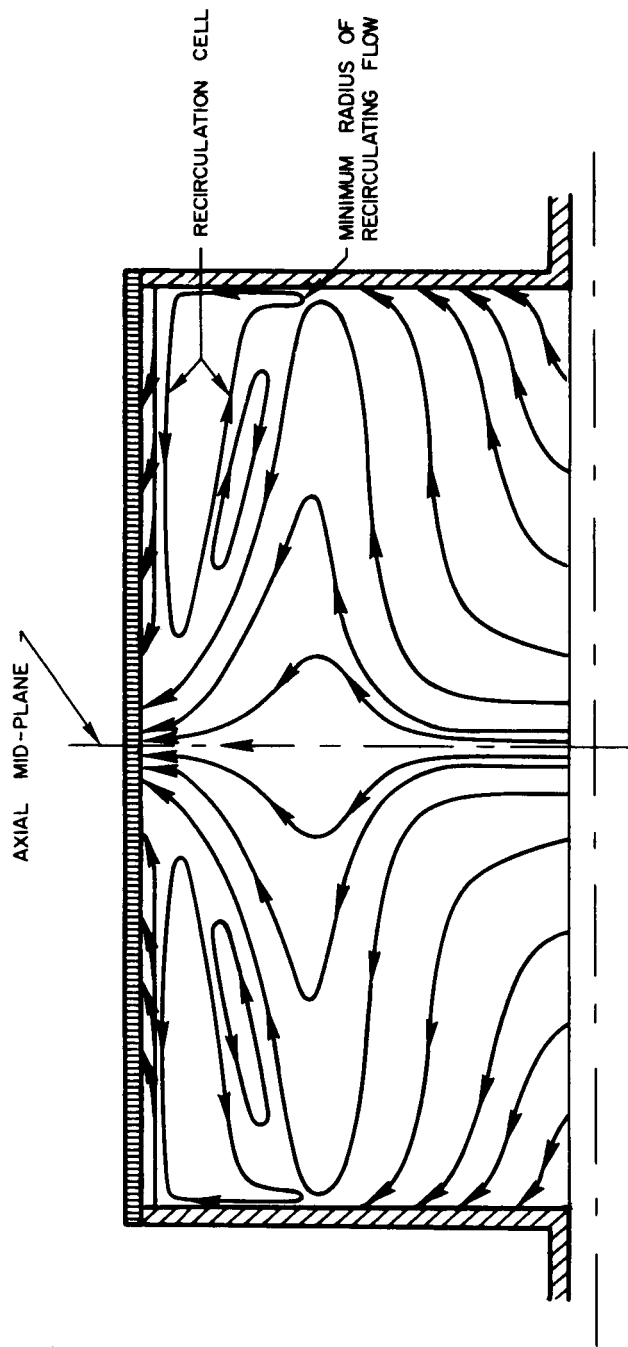


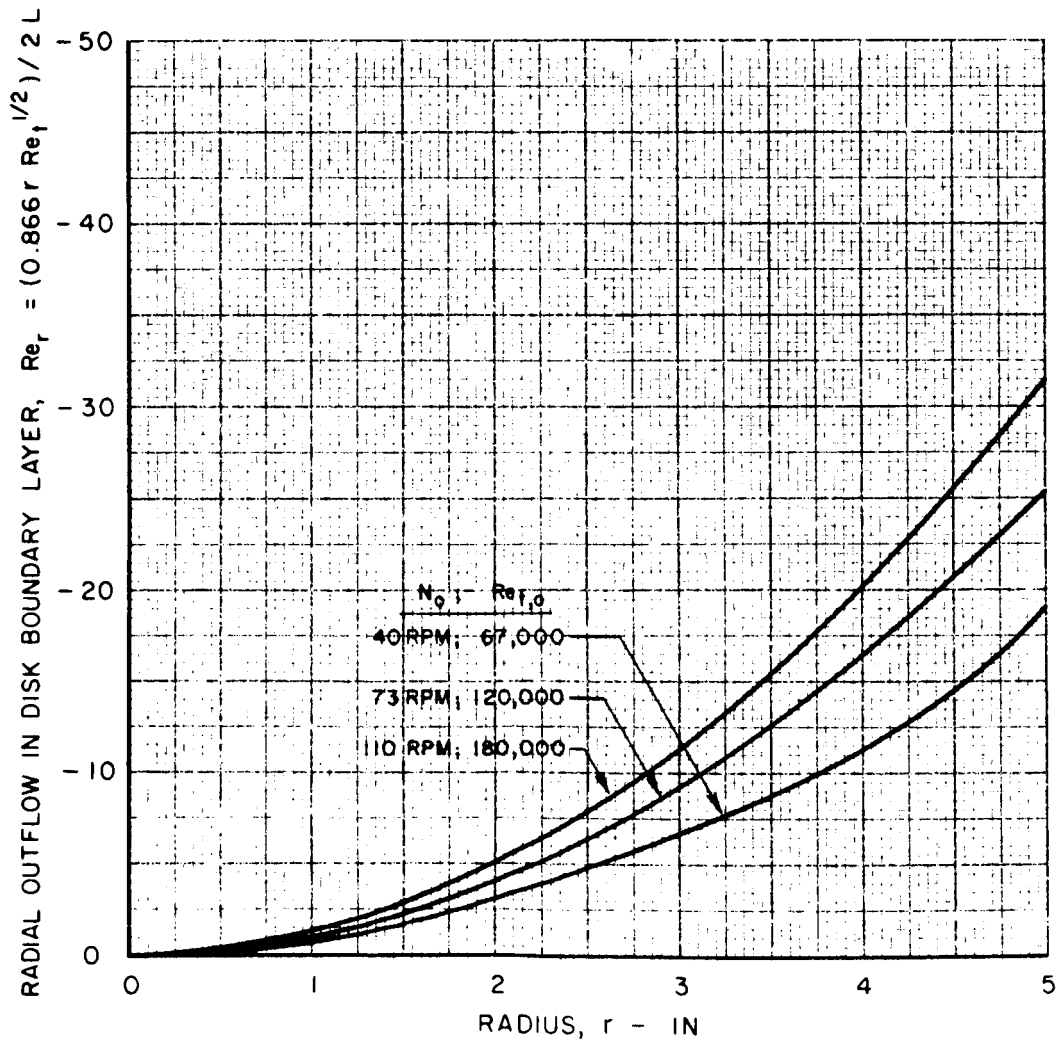
FIG. 17

## RADIAL OUTFLOW IN LAMINAR BOUNDARY LAYER ON A ROTATING DISK

THEORETICAL EQUATION:  $Q_L = 0.886\pi r^3 \omega Re_t^{-1/2}$  FOR FLOW PUMPED RADially OUTWARD BY ROTATING DISK

LETTING  $Q_L = Q_T$  AND SUBSTITUTING IN ABOVE EQUATION,  $Q_T = Re_r 2\pi \nu L$ ;  $\omega = Re_t \nu / r^2$

THUS, FLOW IN BOUNDARY LAYER IN TERMS OF  $Re_r$  IS  $Re_r = 0.886r Re_t^{1/2} / 2L$



EFFECT OF END-WALL ROTATION ON FLOW PATTERNS WITH  
INNER POROUS TUBE AND PERIPHERAL WALL ROTATING  
AT LOW SPEEDS

BASIC VORTEX CONFIGURATION

RADIAL REYNOLDS NUMBER,  $Re_r = -45$   
 FLUID INJECTION THROUGH ROTATING INNER POROUS TUBE  
 PERIPHERAL - WALL SPEED,  $N_o = 73$  RPM  
 TANGENTIAL REYNOLDS NUMBER,  $Re_{t,o} = 120,000$   
 INNER - POROUS - TUBE SPEED,  $N_i = 73$  RPM  
 $N_o / N_i = 1$

FLOW ROTATION

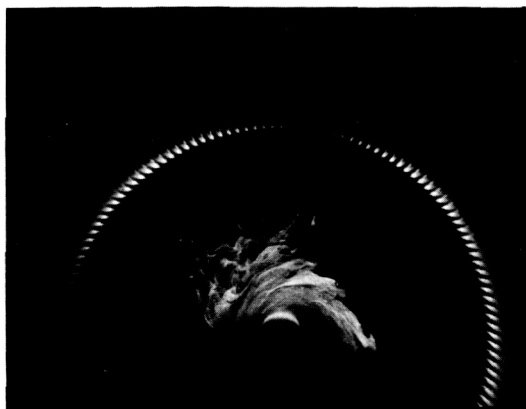


a) STATIONARY END WALLS

b) END WALLS ROTATING WITH PERIPHERAL WALL

DYE NEAR CENTER

DYE NEAR CENTER



DYE NEAR MID-RADIUS

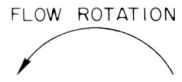
DYE NEAR MID-RADIUS



EFFECT OF END-WALL ROTATION ON FLOW PATTERNS WITH  
 INNER POROUS TUBE AND PERIPHERAL WALL ROTATING  
 AT HIGH SPEEDS

BASIC VORTEX CONFIGURATION

RADIAL REYNOLDS NUMBER,  $Re_r = -45$   
 FLUID INJECTION THROUGH ROTATING INNER POROUS TUBE  
 PERIPHERAL - WALL SPEED,  $N_o = 195$  RPM  
 TANGENTIAL REYNOLDS NUMBER,  $Re_{t,o} = 320,000$   
 INNER - POROUS - TUBE SPEED,  $N_i = 600$   
 $N_o / N_i \approx 0.3$

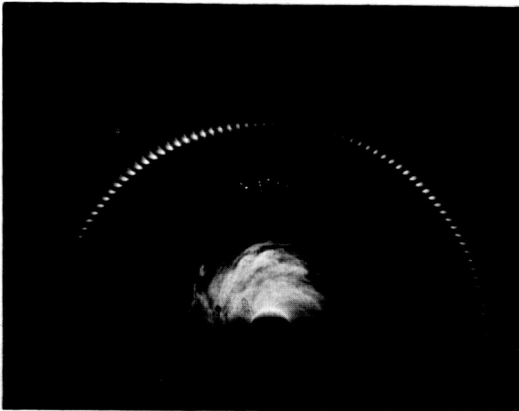


a) STATIONARY END WALLS

b) END WALLS ROTATING WITH PERIPHERAL WALL

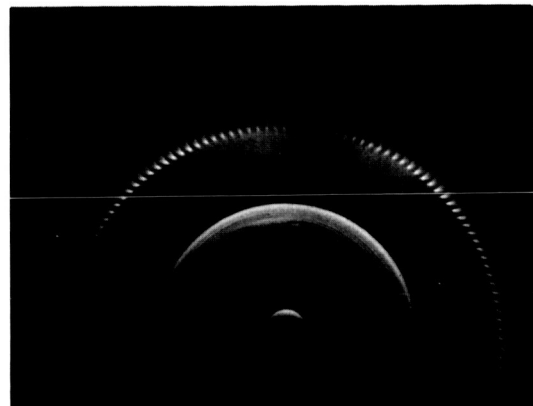
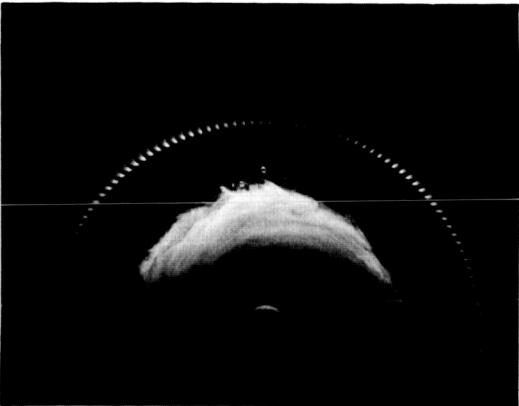
DYE NEAR CENTER

DYE NEAR CENTER



DYE NEAR MID-RADIUS

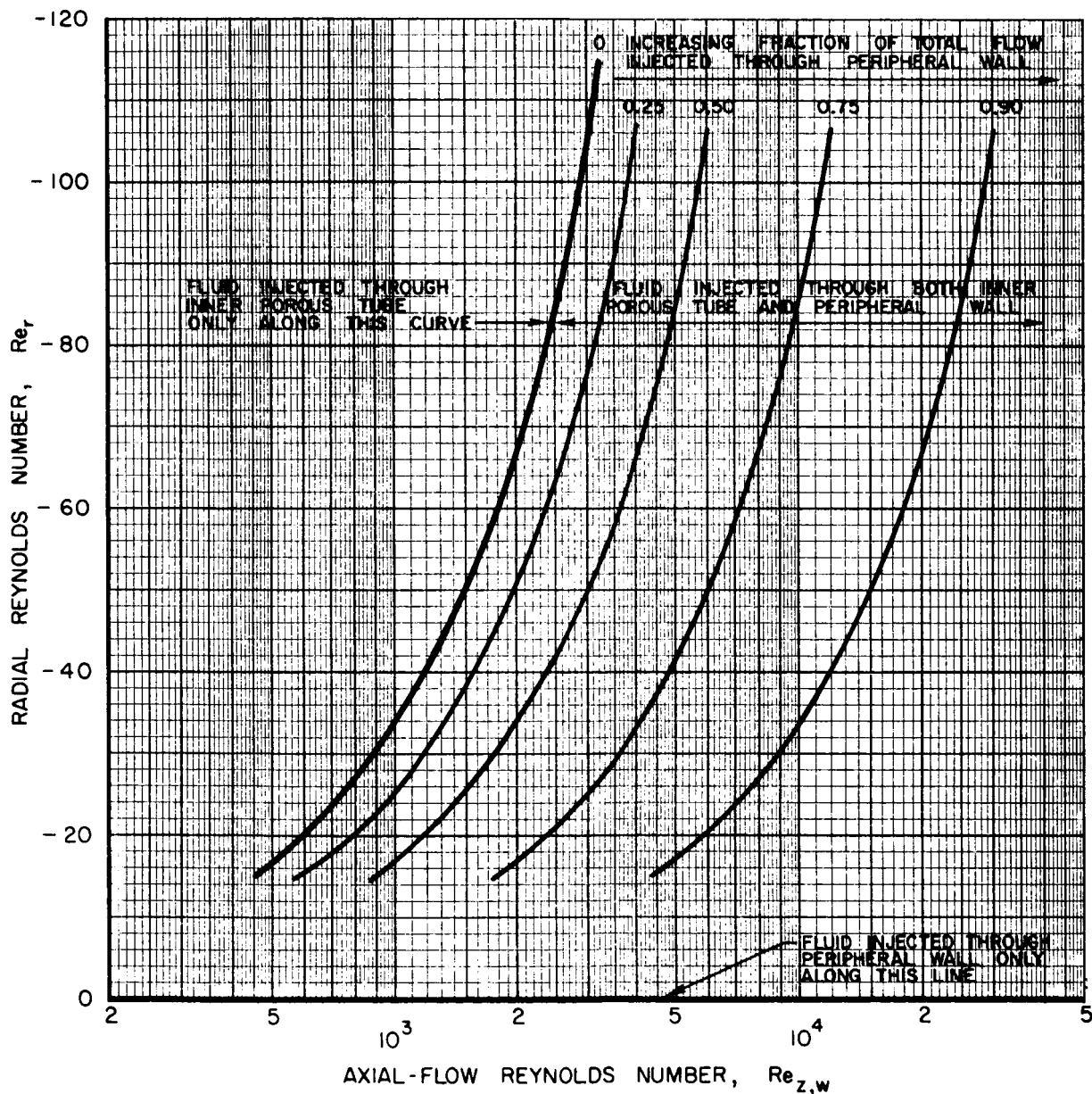
DYE NEAR MID-RADIUS



FRACTION OF TOTAL FLOW INJECTED THROUGH PERIPHERAL WALL  
FOR DIFFERENT COMBINATIONS OF  $Re_r$  AND  $Re_{z,w}$

AXIAL-FLOW VORTEX CONFIGURATION

ROTATING - PERIPHERAL - WALL VORTEX TEST APPARATUS



EFFECT OF END-WALL ROTATION ON FLOW PATTERNS FOR FLUID INJECTION ONLY THROUGH STATIONARY INNER POROUS TUBE

AXIAL-FLOW VORTEX CONFIGURATION

RADIAL REYNOLDS NUMBER,  $Re_r = -45$   
 AXIAL-FLOW REYNOLDS NUMBER,  $Re_{z,w} = 1310$   
 RATIO OF AVERAGE AXIAL VELOCITY TO PERIPHERAL-WALL VELOCITY,  $\bar{V}_{z,w} / V_{\phi,\rho} = 0.0109$   
 PERIPHERAL-WALL SPEED,  $N_0 = 73$  RPM  
 TANGENTIAL REYNOLDS NUMBER,  $Re_{t,0} = 120,000$

FLOW ROTATION



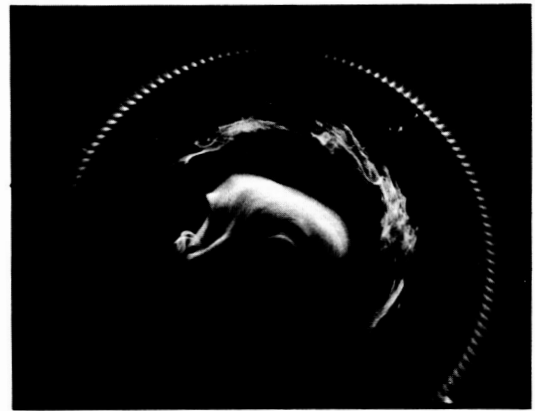
a) STATIONARY END WALLS

DYE NEAR CENTER

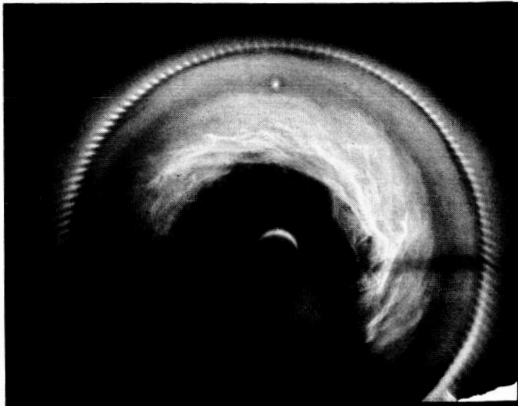


b) ROTATING END WALLS

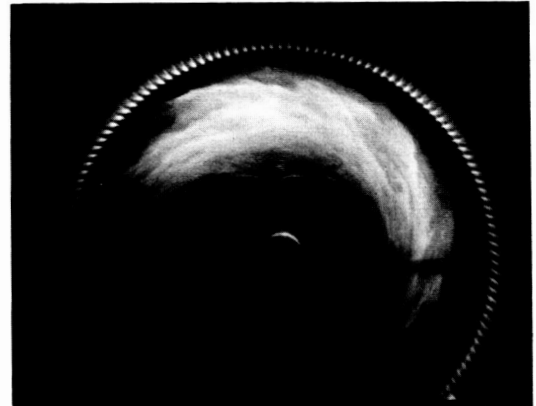
DYE NEAR CENTER



DYE NEAR MID-RADIUS



DYE NEAR MID-RADIUS



EFFECT OF AXIAL-FLOW REYNOLDS NUMBER ON FLOW PATTERNS  
FOR FLUID INJECTION ONLY THROUGH PERIPHERAL WALL

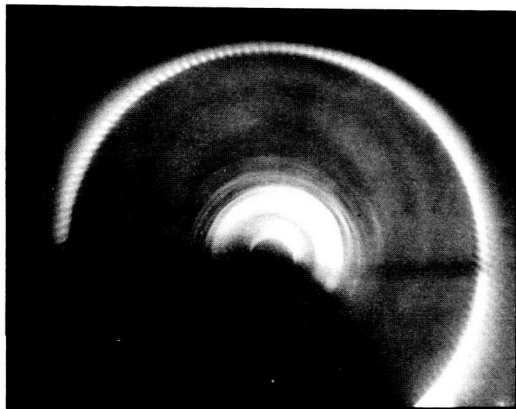
AXIAL-FLOW VORTEX CONFIGURATION

STATIONARY END WALLS  
RADIAL REYNOLDS NUMBER,  $Re_r = 0$   
STATIONARY INNER POROUS TUBE

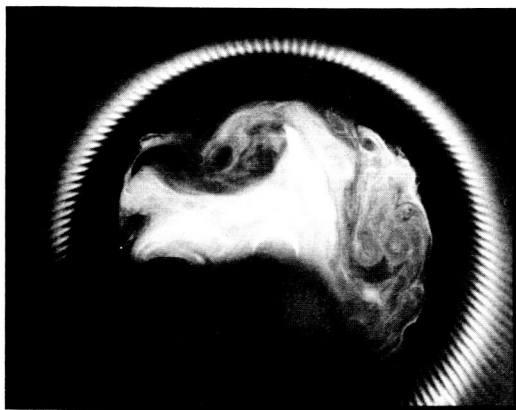
FLOW ROTATION



- a)  $Re_{z,w} = 1310$   
 $\bar{V}_{z,w}/V_{\phi,0} = 0.0109$   
 $N_0 = 73$  RPM  
 $Re_{t,0} = 120,000$



- b)  $Re_{z,w} = 14,000$   
 $\bar{V}_{z,w}/V_{\phi,0} = 0.209$   
 $N_0 = 40$  RPM  
 $Re_{t,0} = 67,000$



- c)  $Re_{z,w} = 21,000$   
 $\bar{V}_{z,w}/V_{\phi,0} = 0.175$   
 $N_0 = 73$  RPM  
 $Re_{t,0} = 120,000$



EFFECT OF AXIAL-FLOW REYNOLDS NUMBER ON FLOW PATTERNS  
WITH FLUID INJECTION THROUGH BOTH PERIPHERAL WALL AND  
STATIONARY INNER POROUS TUBE

AXIAL-FLOW VORTEX CONFIGURATION

STATIONARY END WALLS-

RADIAL REYNOLDS NUMBER,  $Re_r = -45$

SEE FIG. 21 FOR FRACTION OF FLOW INJECTED THROUGH PERIPHERAL WALL

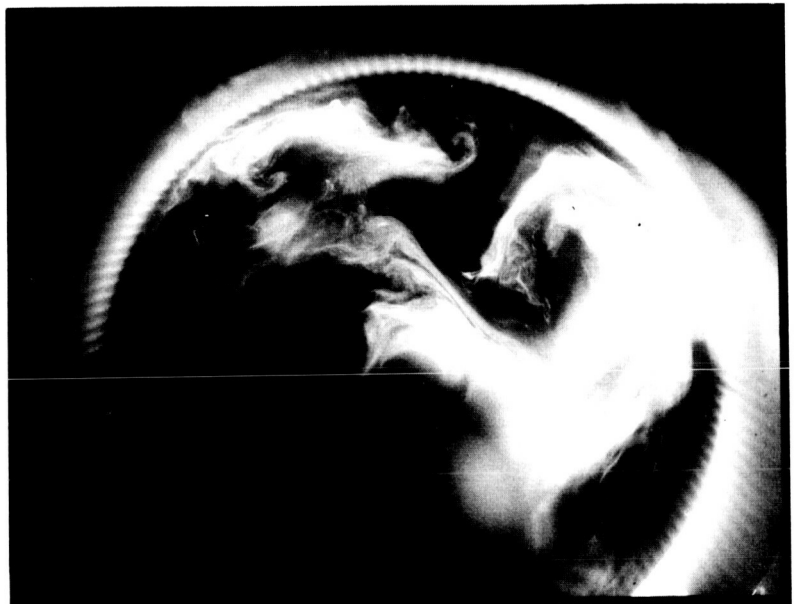
FLOW ROTATION



- a)  $Re_{z,w} = 2620$   
 $\bar{V}_{z,w} / V_{\phi,o} = 0.0109$   
 $N_o = 144 \text{ RPM}$   
 $Re_{t,o} = 240,000$



- b)  $Re_{z,w} = 14,000$   
 $V_{z,w} / V_{\phi,o} = 0.0745$   
 $N_o = 112 \text{ RPM}$   
 $Re_{t,o} = 188,000$



EFFECTS OF AXIAL-FLOW REYNOLDS NUMBER AND FLUID INJECTION METHOD  
ON FLOW PATTERNS WITH INNER POROUS TUBE ROTATING

FIG. 25

AXIAL-FLOW VORTEX CONFIGURATION

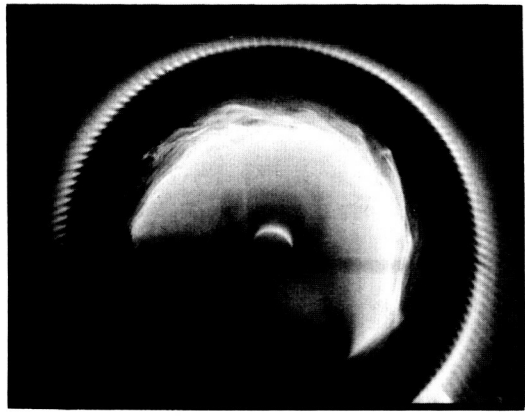
ROTATING END WALLS

FLOW ROTATION



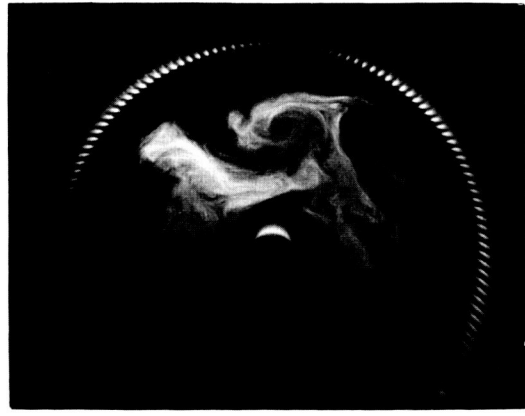
a) FLUID INJECTION ONLY THROUGH ROTATING INNER POROUS TUBE

$Re_{z,w} = 1310$   
 $\bar{V}_{z,w}/V_{\phi,0} = 0.0109$   
 $Re_r = -45$   
 $N_o = 73 \text{ RPM}$   
 $Re_{t,0} = 120,000$   
 $N_i = 500 \text{ RPM}$



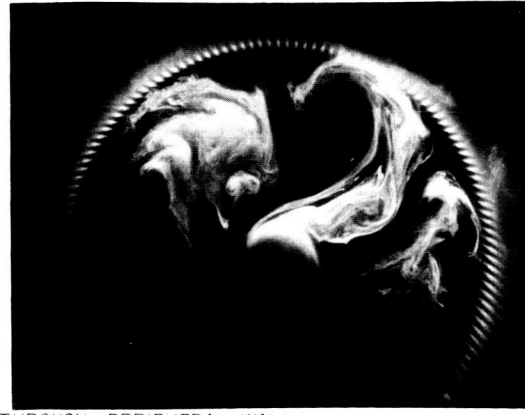
b) FLUID INJECTION ONLY THROUGH PERIPHERAL WALL

$Re_{z,w} = 21,000$   
 $\bar{V}_{z,w}/V_{\phi,0} = 0.175$   
 $Re_r = 0$   
 $N_o = 73 \text{ RPM}$   
 $Re_{t,0} = 120,000$   
 $N_i = 500 \text{ RPM}$



c) FLUID INJECTION THROUGH BOTH PERIPHERAL WALL AND INNER POROUS TUBE \*

$Re_{z,w} = 14,000$   
 $\bar{V}_{z,w}/V_{\phi,0} = 0.0498$   
 $Re_r = -45$   
 $N_o = 168 \text{ RPM}$   
 $Re_{t,0} = 280,000$   
 $N_i = 600 \text{ RPM}$



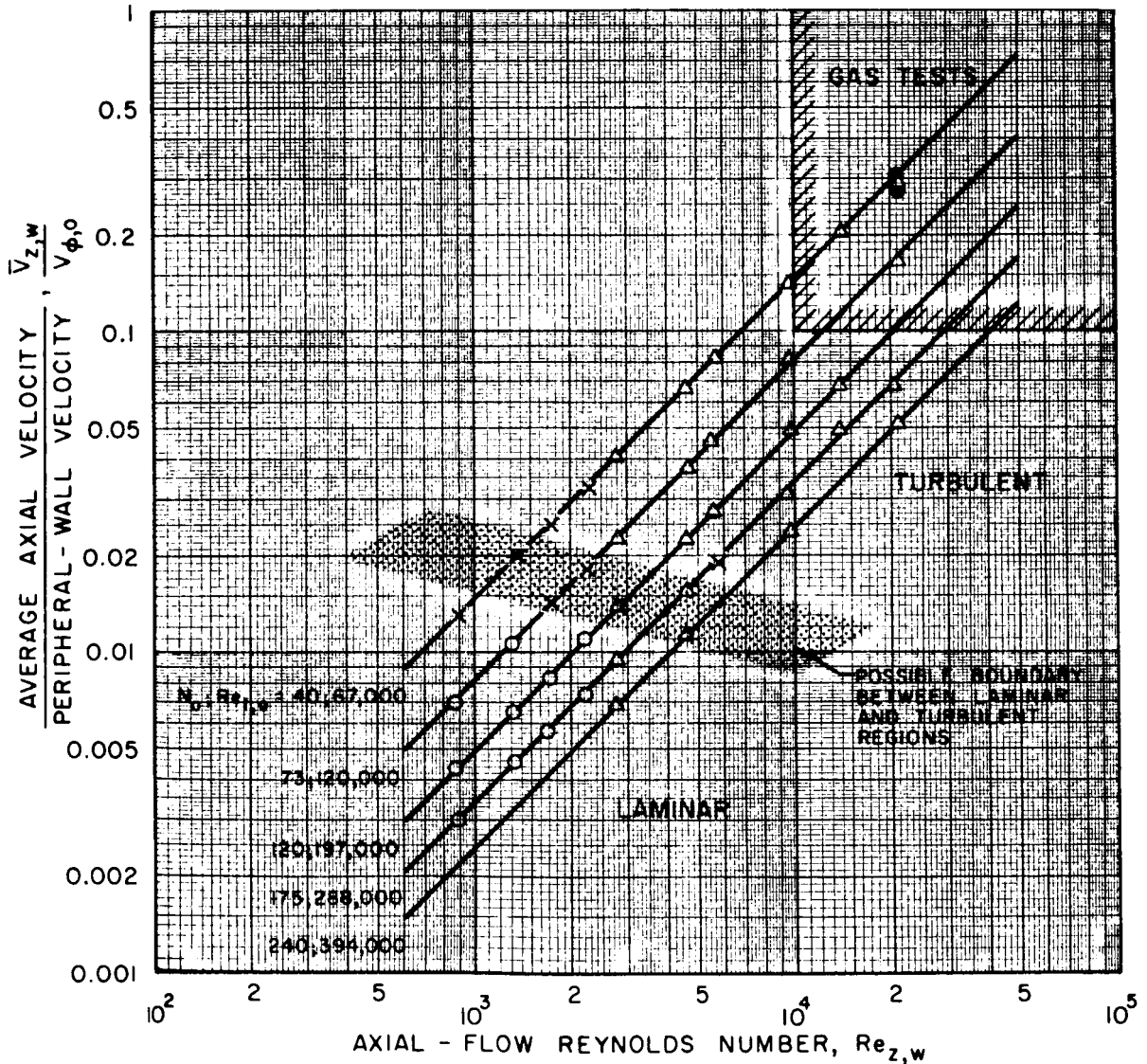
\*SEE FIG. 21 FOR FRACTION OF FLOW INJECTED THROUGH PERIPHERAL WALL

SUMMARY OF LAMINAR AND TURBULENT FLOW CONDITIONS  
OBSERVED IN AXIAL-FLOW VORTEX CONFIGURATION

ROTATING-PERIPHERAL-WALL VORTEX TEST APPARATUS

BOTH STATIONARY AND ROTATING END WALLS  
STATIONARY INNER POROUS TUBE  
ALL VALUES OF RADIAL REYNOLDS NUMBER,  $Re_r$

SYMBOL	TYPE FLOW
○	LAMINAR IN CENTRAL REGION
△	TURBULENT
×	OSCILLATING LAMINAR AND TURBULENT
●	RADIAL INFLOW, LAMINAR



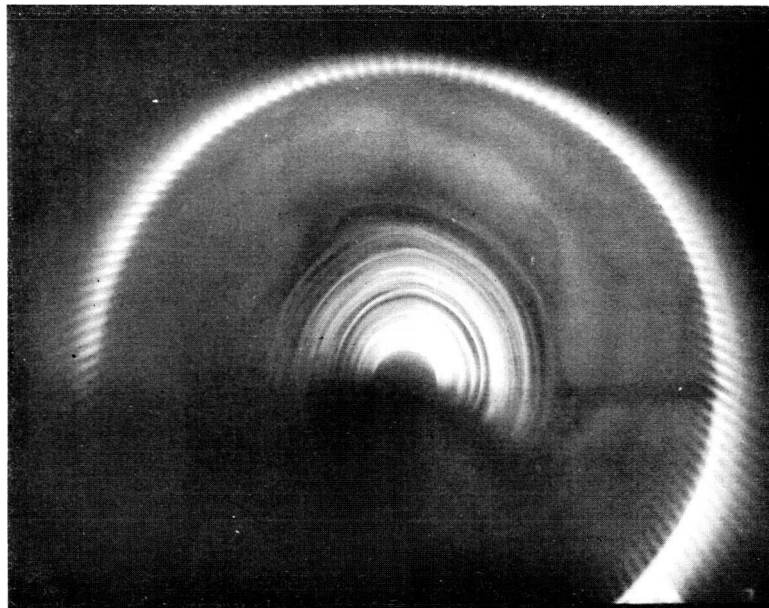
TYPICAL OSCILLATING LAMINAR AND TURBULENT FLOW PATTERNS  
 AXIAL-FLOW VORTEX CONFIGURATION

SEE FIG. 26 FOR COMBINATIONS OF  $Re_{z,w}$  AND  $\bar{V}_{z,w}/V_{\phi,0}$  LEADING TO THESE FLOW PATTERNS  
 FLOW RETURNS TO PATTERN a) AFTER APPROXIMATELY 45 SEC IN PATTERN b)

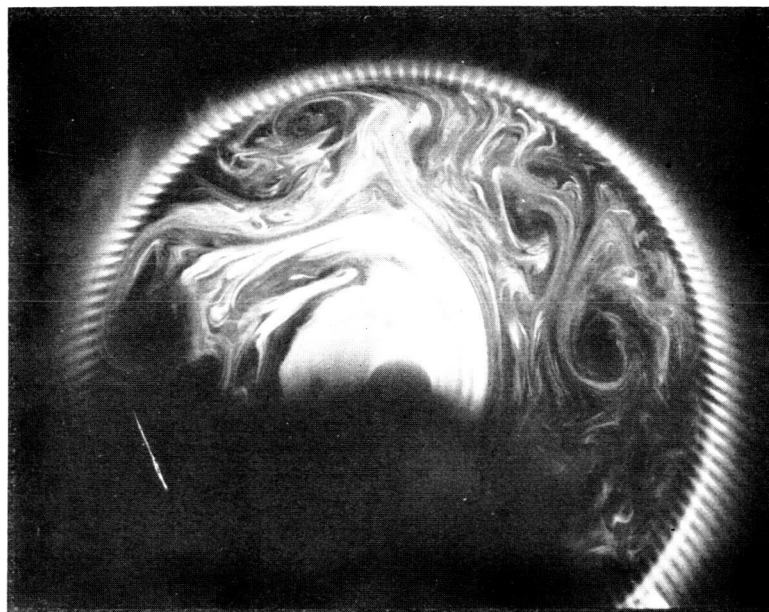
FLOW ROTATION



a) BEFORE ONSET OF LARGE EDDIES



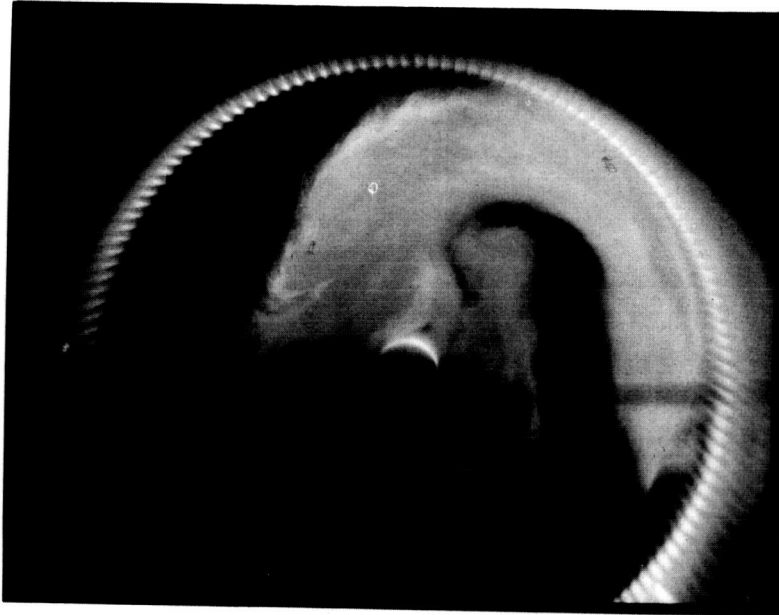
b) AFTER ONSET OF LARGE EDDIES



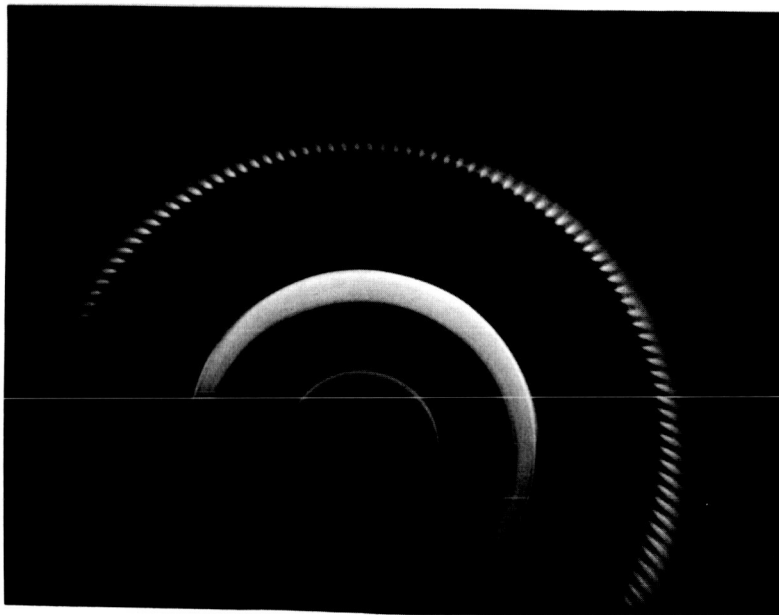
COMPARISON OF TYPICAL RADIAL OUTFLOW AND RADIAL INFLOW  
FLOW PATTERNS IN ROTATING-PERIPHERAL-WALL VORTEX  
TEST APPARATUS

AXIAL-FLOW VORTEX CONFIGURATION

- a) RADIAL OUTFLOW:  $Re_{z,w} = 14,000$ ,  $\bar{V}_{z,w}/V_{t,0} = 0.15$ ,  $Re_r = -45$ ,  $N_0 = 56$  RPM,  $Re_{t,0} = 93,000$ ;  
FLUID INJECTION THROUGH STATIONARY INNER POROUS TUBE



- b) RADIAL INFLOW:  $Re_{z,w} = 16,000$ ,  $\bar{V}_{z,w}/V_{t,0} = 0.25$ ,  $Re_r = 90$ ,  $N_0 = 40$  RPM,  $Re_{t,0} = 67,000$ ;  
FLUID INJECTION THROUGH PERIPHERAL WALL AND FLUID WITHDRAWAL  
THROUGH THRU-FLOW PORTS AT CENTERS OF END WALLS

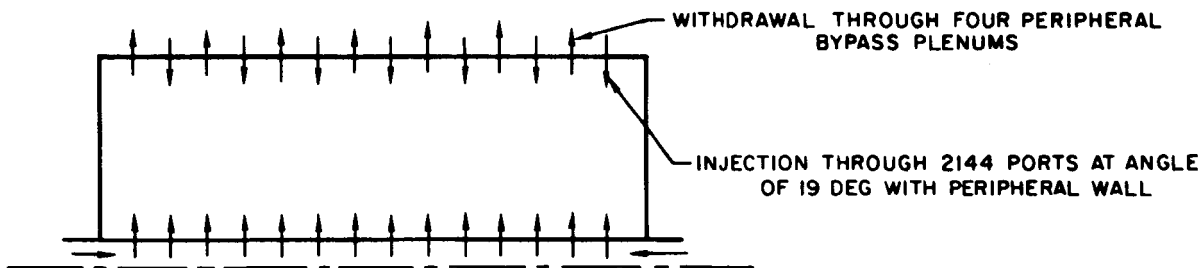


# SKETCHES OF FLUID INJECTION METHODS USED IN 2144-PORT-INJECTION VORTEX TUBE

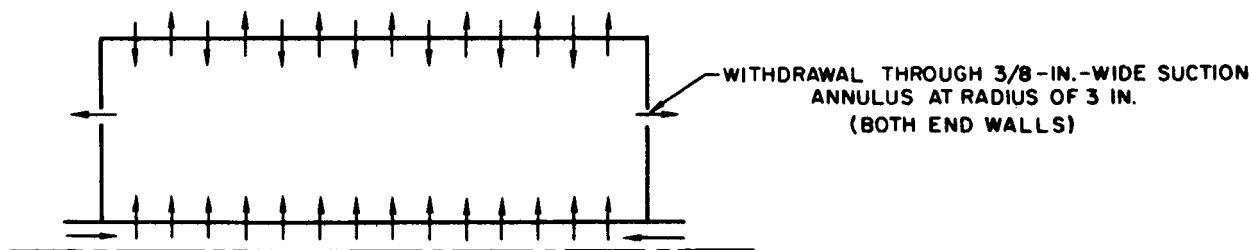
NOTE: FLUID WAS ALSO INJECTED THROUGH PERIPHERAL WALL IN ALL CONFIGURATIONS SHOWN BELOW

## a) BASIC VORTEX CONFIGURATION

FLUID INJECTION THROUGH INNER POROUS TUBE

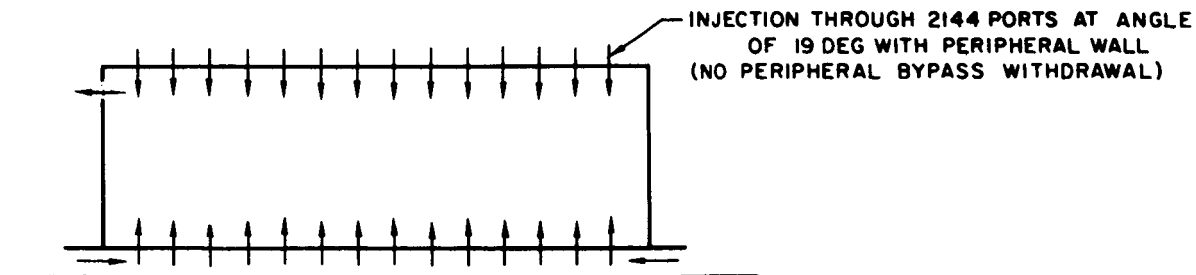


FLUID INJECTION THROUGH INNER POROUS TUBE AND END-WALL SUCTION

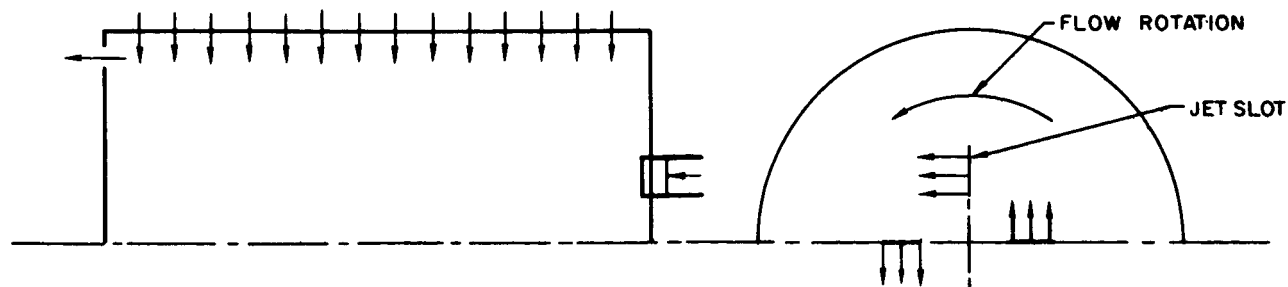


## b) AXIAL-FLOW VORTEX CONFIGURATION

FLUID INJECTION THROUGH INNER POROUS TUBE



TANGENTIAL FLUID INJECTION THROUGH FOUR 1-IN.-LONG JET SLOTS AT NONAXIAL-FLOW END WALL  
(SLOT EXTENDING FROM  $r = 0.75$  IN. TO  $r = 1.75$  IN.)



EFFECT OF INNER POROUS TUBE ROTATION ON FLOW PATTERNS  
IN 2144-PORT-INJECTION VORTEX TUBE

BASIC VORTEX CONFIGURATION

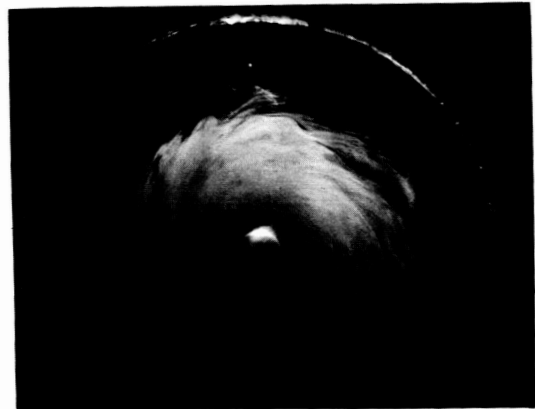
RADIAL REYNOLDS NUMBER,  $Re_r = -60$   
 FLUID INJECTION THROUGH INNER POROUS TUBE  
 TANGENTIAL INJECTION REYNOLDS NUMBER,  $Re_{t,j} = 120,000$   
 TANGENTIAL INJECTION VELOCITY,  $V_j = 3.16$  FT/SEC

FLOW ROTATION



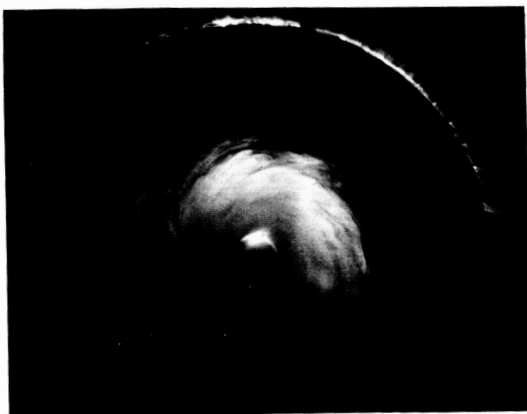
a) INNER POROUS TUBE SPEED,  $N_i = 0$  RPM

b) INNER POROUS TUBE SPEED,  $N_i = 400$  RPM



c) INNER POROUS TUBE SPEED,  $N_i = 1200$  RPM

d) INNER POROUS TUBE SPEED,  $N_i = 2000$  RPM



EFFECT OF INNER POROUS TUBE ROTATION ON TANGENTIAL VELOCITY PROFILES IN 2144-PORT-INJECTION VORTEX TUBE

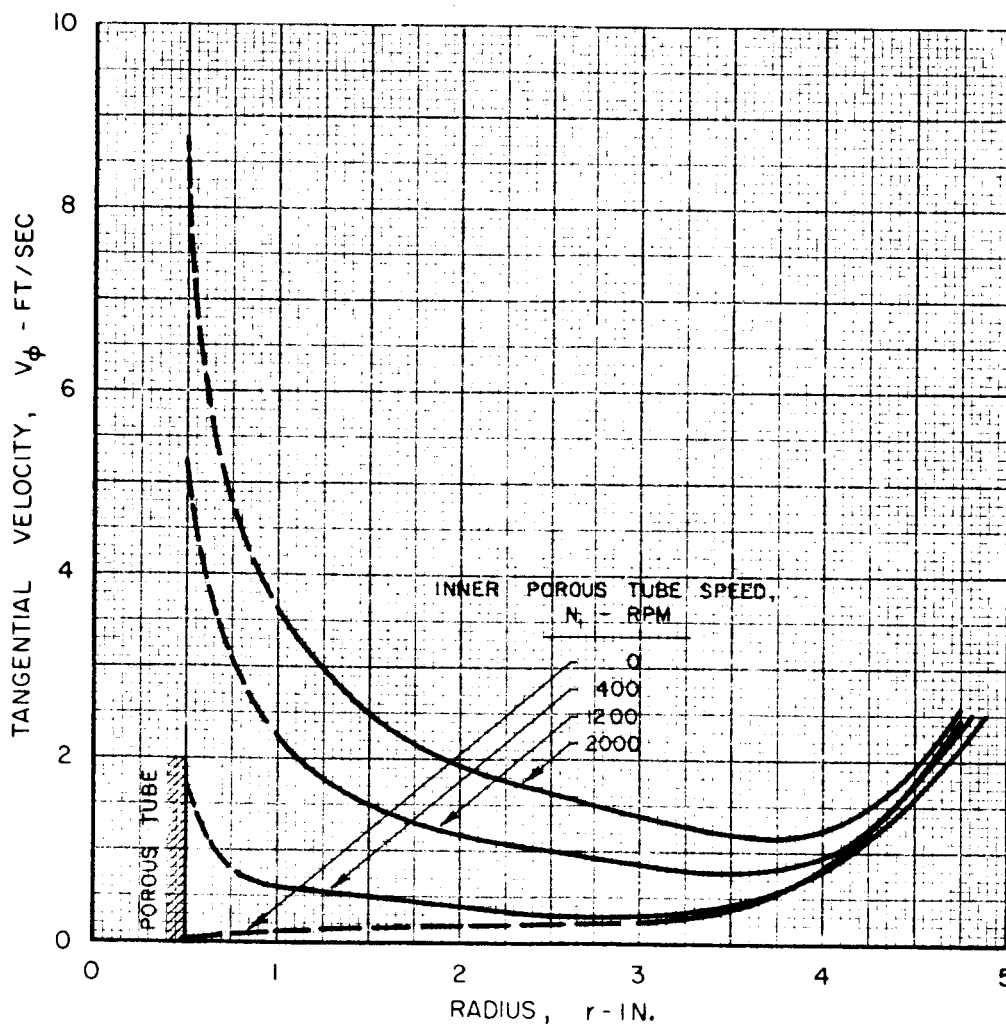
BASIC VORTEX CONFIGURATION

RADIAL REYNOLDS NUMBER,  $Re_r = -30$

FLUID INJECTION THROUGH INNER POROUS TUBE

TANGENTIAL INJECTION REYNOLDS NUMBER,  $Re_{t,j} = 120,000$

TANGENTIAL INJECTION VELOCITY,  $v_j = 3.16$  FT/SEC



TYPICAL MULTIPLE-VORTEX FLOW PATTERNS IN 2144-PORT-  
INJECTION VORTEX TUBE WITH FLOW WITHDRAWAL THROUGH  
END - WALL SUCTION ANNULUS

BASIC VORTEX CONFIGURATION

TANGENTIAL INJECTION REYNOLDS NUMBER,  $Re_{t,j} = 120,000$

TANGENTIAL INJECTION VELOCITY,  $v_j = 3.16$  FT/SEC

SEE FIG.29 FOR DETAILS OF SUCTION ANNULUS CONFIGURATION

a) END-WALL SUCTION RADIAL REYNOLDS NUMBER,  $Re_{r,s} = 135$

FLOW ROTATION  
  
 $Re_r = -45$   
 $N_i = 0$  RPM



b) END-WALL SUCTION RADIAL REYNOLDS NUMBER,  $Re_{r,s} = 75$

FLOW ROTATION  
  
 $Re_r = 0$   
 $N_i = 800$  RPM



# TYPICAL TANGENTIAL VELOCITY PROFILES IN 2144-PORT-INJECTION VORTEX TUBE WITH FLOW WITHDRAWAL THROUGH END-WALL SUCTION ANNULUS

## BASIC VORTEX CONFIGURATION

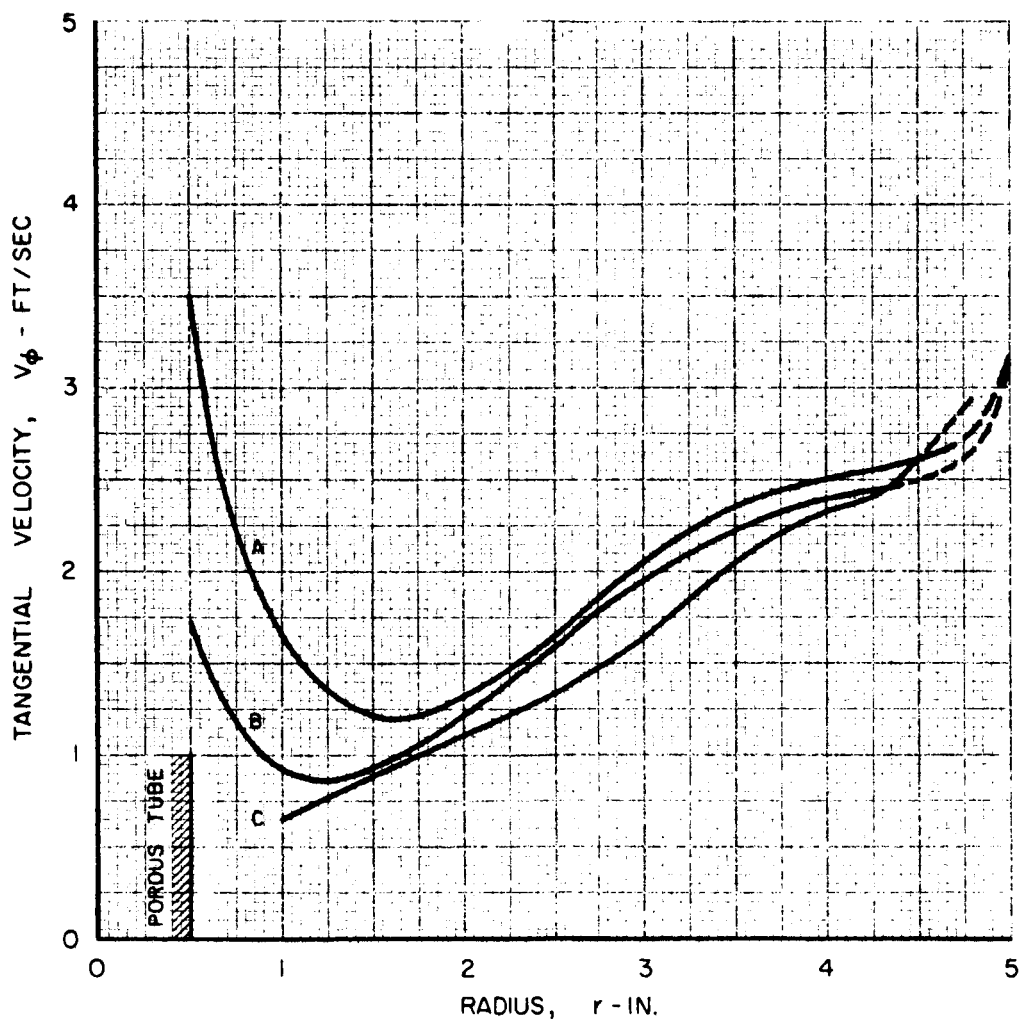
TANGENTIAL INJECTION REYNOLDS NUMBER,  $Re_{t,i} = 120,000$

TANGENTIAL INJECTION VELOCITY,  $v_j = 3.16$  FT/SEC

SEE FIG. 29a FOR DETAILS OF SUCTION ANNULUS CONFIGURATION

CURVE	$Re_{r,s}$	$Re_r$	$N_i$ - RPM
A*	75	0	800
B	75	0	400
C*	135	-45	0

\*SEE PHOTOGRAPHS IN FIG. 32



# COMBINATIONS OF FLOW CONDITIONS THAT PRODUCE MULTIPLE-VORTEX FLOW PATTERNS

## BASIC VORTEX CONFIGURATION

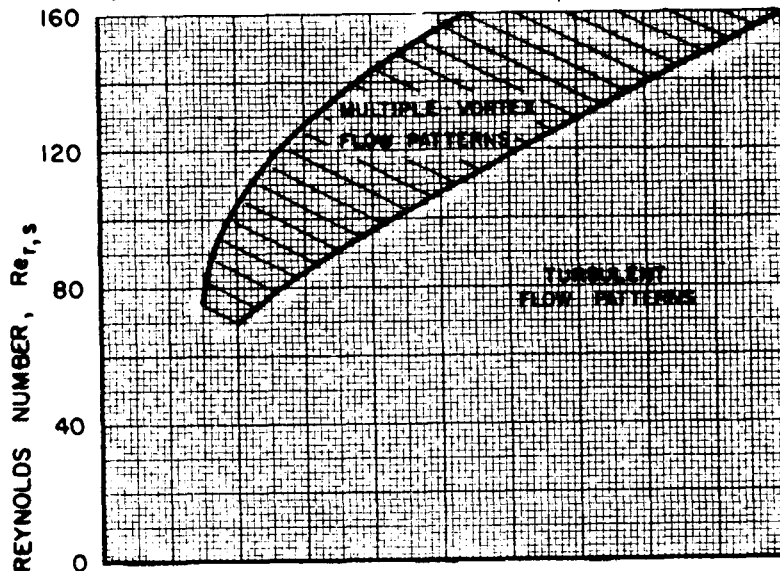
2144-PORT-INJECTION VORTEX TUBE WITH END-WALL SUCTION ANNULUS

TANGENTIAL INJECTION REYNOLDS NUMBER,  $Re_{t,i} = 120,000$

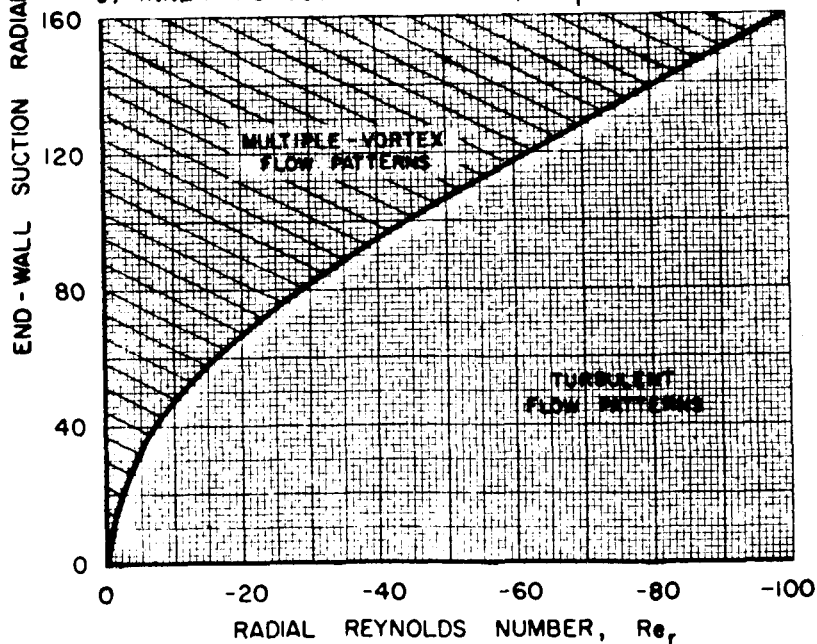
TANGENTIAL INJECTION VELOCITY,  $V_i = 3.16$  FT/SEC

SEE FIG. 29a FOR DETAILS OF SUCTION ANNULUS CONFIGURATION

a) INNER POROUS TUBE SPEED,  $N_i = 0$  RPM



b) INNER POROUS TUBE SPEED,  $N_i = 800$  RPM



# EFFECT OF INNER POROUS TUBE ROTATION ON MULTIPLE-VORTEX FLOW PATTERNS

## BASIC VORTEX CONFIGURATION

2144-PORT-INJECTION VORTEX TUBE WITH END-WALL SUCTION ANNULUS  
 TANGENTIAL INJECTION REYNOLDS NUMBER,  $Re_{t,j} = 120,000$   
 TANGENTIAL INJECTION VELOCITY,  $V_j = 3.16$  FT/SEC  
 RADIAL REYNOLDS NUMBER,  $Re_r = -75$   
 END-WALL SUCTION RADIAL REYNOLDS NUMBER,  $Re_{r,s} = 150$

SEE FIG. 29a FOR DETAILS OF SUCTION ANNULUS CONFIGURATION

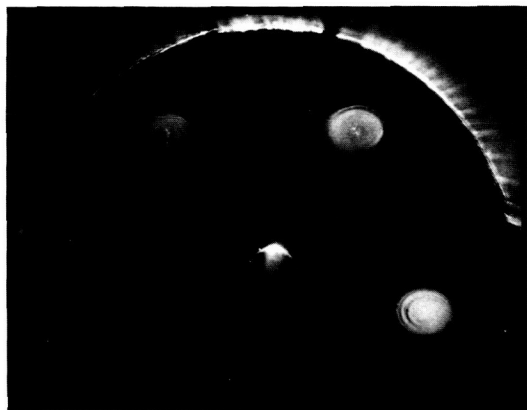
FLOW ROTATION



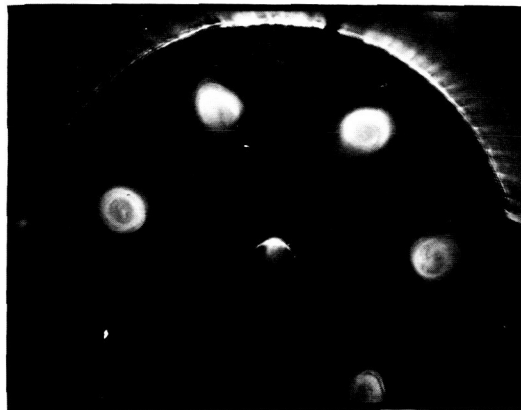
a) INNER POROUS TUBE SPEED,  $N_i = 400$  RPM



b) INNER POROUS TUBE SPEED,  $N_i = 800$  RPM



c) INNER POROUS TUBE SPEED,  $N_i = 1200$  RPM



EFFECT OF TANGENTIAL INJECTION THROUGH SLOTS IN NONAXIAL-FLOW END WALL ON FLOW PATTERNS IN 2144-PORT-INJECTION VORTEX TUBE

AXIAL-FLOW VORTEX CONFIGURATION

RADIAL REYNOLDS NUMBER,  $Re_r = 0$   
 NO INNER POROUS TUBE  
 TANGENTIAL INJECTION REYNOLDS NUMBER,  $Re_{t,j} = 120,000$   
 TANGENTIAL INJECTION VELOCITY,  $V_j = 3.16$  FT/SEC  
 SEE FIG. 29b FOR DETAILS OF END-WALL INJECTION CONFIGURATION

FLOW ROTATION



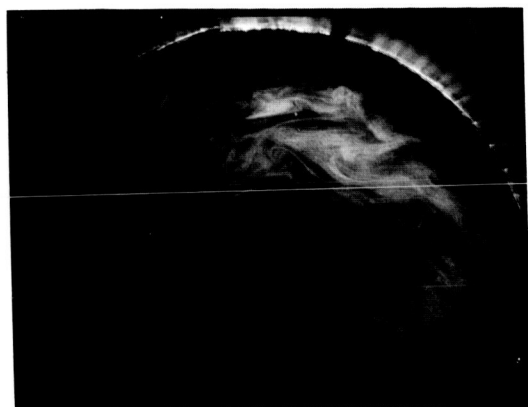
a) END-WALL INJECTION RADIAL REYNOLDS NUMBER,  $Re_{r,i} = 0$



b) END-WALL INJECTION RADIAL REYNOLDS NUMBER,  $Re_{r,i} = 25$



c) END-WALL INJECTION RADIAL REYNOLDS NUMBER,  $Re_{r,i} = 50$



d) END-WALL INJECTION RADIAL REYNOLDS NUMBER,  $Re_{r,i} = 80$

